Lab on a Chip

ROYAL SOCIETY OF CHEMISTRY

CRITICAL REVIEW

View Article Online
View Journal | View Issue

Cite this: *Lab Chip*, 2026, **26**, 1273

20 years of microfluidic technology for advancing plant sciences

Louis D. Cohen, Eleonora Moratto and Claire E. Stanley *

Understanding how plants respond to dynamic and spatially variable stimuli is a key goal in plant sciences. Traditional imaging methods often involve a trade-off between environmental control and spatial resolution, limiting their ability to capture real-time responses in high resolution. Microfluidic technology overcomes these limitations by facilitating precise control of environmental conditions and high-resolution live imaging. In the past two decades, microfluidic technology has increasingly been applied in plant sciences research. This review summarises current applications of microfluidic technology in plant sciences, including studies of root–rhizosphere interactions, tip-growing plant cells, plant protoplasts, and plant phenotyping. Emerging trends are explored, and key research gaps are highlighted.

Received 7th November 2025,
Accepted 3rd February 2026

DOI: 10.1039/d5lc01036e

rsc.li/loc

1 Introduction

Plants must constantly react to environmental cues, requiring a high degree of phenotypic plasticity. How plants achieve this plasticity at different spatial and temporal scales remains an open question in plant sciences: how do plant roots respond to temporally and spatially heterogeneous chemical environments? How do plant roots interact with the soil microbiome at different scales? How do plant cells sense and respond to heterogeneous chemical environments, grow, and develop into complex multicellular organisms? Answering these questions requires precise control of plants' biotic and abiotic environments, combined with high-resolution spatial and temporal imaging of plants. Implementation of classical agar-based approaches[1–3] to answer these questions is limited, due to coarse environmental control at the plate scale, and low-resolution imaging. Hence, microfluidic technology aims to fill this methodological gap. As a result, microfluidic technology has been increasingly utilised in the plant and wider biological sciences over the past two decades, having been adapted from its original use in the chemical sciences for the manipulation of very small fluid volumes (fL–nL) to

Department of Bioengineering, Imperial College London, London, SW7 2AZ, UK.
E-mail: claire.stanley@imperial.ac.uk

Louis Cohen

Louis Cohen is a PhD candidate in the Department of Bioengineering at Imperial College London. He earned his undergraduate degree in Plant Sciences from the University of Cambridge, graduating with the top first-class degree and receiving the T.B. Woods Prize. His current research focuses on exploring root–fungal interactions at single-cell resolution using microfluidic technology.

Eleonora Moratto

Eleonora Moratto is a postdoctoral researcher in the Department of Bioengineering at Imperial College London. In 2024, she received her PhD in plant–pathogen interactions from the Department of Life Sciences at Imperial. During her PhD, she was awarded the Laura Bassi Scholarship (2023) and was nominated Woman Scientist of the Month by the European Platform of Women Scientists (2023). Eleonora is also the Early Career Researcher representative for the Imperial Fungal Science Network. Her current research focuses on bacterial dispersal on so-called "fungal highways" using microfluidic technology and image analysis techniques.

perform chemical reactions with precise control and in a high-throughput manner.[4]

Microfluidic devices are customised microenvironments that have at least one dimension less than one millimetre in size. They are often manufactured from transparent materials and exploit thin optical interfaces to facilitate high-resolution imaging of the enclosed samples. Inclusion of customised internal microstructures and control over fluid perfusion facilitate precise control and measurement of the internal microenvironment. This technology, sometimes referred to as lab-on-a-chip (LOC),[5] "chip" technology, or micro-electromechanical (MEMS) systems,[6] will be henceforth referred to as microfluidic technology, and associated microfluidic devices. Emerging from the use of microfluidic technology for the study of single cells, such as yeast[7–9] and bacteria,[7,10,11] the field of plant microfluidics was founded in 2006 with the development of a microfluidic device for trapping tobacco protoplasts[12] and later expanded to the study of root-environment interactions with the "RootChip" devices from 2010 onwards.[13] Today, the field of plant microfluidics encompasses many areas of plant biology, from plant–microbe interactions to high-throughput phenotyping of plant cells and seedlings.

To date, several reviews[14–17] have been explored the application of microfluidic technology to plant sciences, but to date no single review has attempted to synthesise all existing research concerning the application of microfluidic technology to plant sciences. This review aims both to update the field, and to summarise all research that uses microfluidic technology to advance the field of plant sciences, encompassing research from 2006 to 2025. Microfluidic devices for plant sciences can be categorised by the type of biological question the microfluidic device has been designed to answer, which in turn determines device and experimental design. Therefore, we categorise existing research into microfluidic device-assisted: i) imaging of root–rhizosphere interactions, ii) imaging of tip-growing plant cells, iii) imaging and manipulation of single or small groups of plant cells, and iv) plant phenotyping. Current trends in the field and future directions of research are discussed, with a focus on novel microfluidic device designs and fabrication methods.

Claire Stanley

Claire Stanley is an Associate Professor in the Department of Bioengineering at Imperial College London, where she leads the Microbiome, Microscopy and Microfluidics lab. She received her PhD in Chemistry from Imperial and conducted postdoctoral research at ETH Zurich. In 2016, she was awarded a prestigious SNSF Ambizione Fellowship to start her independent research team at Agroscope and became a Lecturer at Imperial in 2020. Her lab works on the development and application of microfluidic technology for projects positioned at the interface between bioengineering, fungal science and plant biology. Claire is also co-director of the Imperial Fungal Science Network.

2 Microfluidic device-assisted imaging of root–rhizosphere interactions

Plant scientists have studied the relationship between plant roots and the rhizosphere for decades, and we now appreciate rhizospheric environments to be one of the most dynamic and heterogeneous environments on Earth.[18] Plant roots are required to be phenotypically plastic to respond to this environmental dynamism and heterogeneity. Understanding phenotypic plasticity requires observation of plant phenotypes as a response to changing chemical, biological, and physical stimuli at multiple spatial and temporal scales. Classical approaches involve growing roots on agar plates and measuring the impact of the chemical, biological or physical agents on various root phenotypes such as root development, physiology, cytology, and gene expression.[19] This approach has yielded valuable insights, such as the impact of nutrient deficiencies on *Arabidopsis thaliana* root plasticity,[20] but there are several limitations to this approach. Firstly, high-resolution imaging of root development is not possible due to the thickness and opacity of agar. This limits the use of high numerical aperture objective lenses with short working distances, and roots grow out of focus due to gravitropic-induced bending. Secondly, classical approaches can achieve only coarse spatial control of chemical and biological agents, whereas plant developmental processes can be influenced on the micrometre scale. Microfluidic technology offers a way to overcome these limitations. Firstly, customisable microchannel heights facilitate focal confinement of the root, allowing high-resolution images to be taken over long time periods. Secondly, control of fluid perfusion combined with custom microchamber and microchannel geometries results in fine spatial and temporal control of the internal microenvironment. Finally, microfluidic technology can leverage other complementary technologies to probe further into root dynamics. For example, genetically encoded biosensors such as Förster resonance energy transfer (FRET) biosensors[21] can provide information on intracellular metabolites and ions of individual plant cells in real time. In this section, the application of microfluidic technology for the investigation of root–rhizosphere interactions will be

explored including: i) root–chemical, ii) root–microbe, and iii) root–physical interactions.

2.1 Microfluidic technology facilitates high-resolution imaging of roots

Microfluidic devices are typically used to image plant roots by growing a primary root inside a microchannel with dimensions customised for the average diameter of the primary root of the plant being studied. This confines the growth of the primary root to a single focal plane, and aids root growth in a direction amenable to study. Seeds or seedlings (where seeds are germinated off-chip) are inoculated into microfluidic devices to image the growing root from a few days[22] to over a month[23] after germination. The first microfluidic devices developed to image primary roots consisted of a single straight microchannel to confine the primary root of a dicotyledonous plant such as *A. thaliana* (Fig. 1A–C). Device design progressed from confining the root apex,[13] to the whole root or seedling[22,24–28] inside the microchannel. This increased integration of the root into the microfluidic device facilitates longer experiments, as a smaller proportion of the root surface area is exposed to desiccation and nutrient depletion zones.[29] Longer experiments are important for facilitating the study of later stages of plant development, and to study plants with longer lifecycles such as tree seedlings.[23] For plants with root diameters less than 200 μm, such as *A. thaliana*, photolithography is an appropriate technique to fabricate the microchannels. However, it is difficult to use this technique for manufacturing channels heights larger than 200 μm. As most economically important crop plants possess roots with diameters more than 200 μm, other microfabrication techniques have been employed to focally confine larger root systems of plants such as rice (*Oryza sativa*),[24] *Brachypodium distachyon*[30] and hemp (*Cannabis sativa*).[31] For example, channel heights of 300 μm have been fabricated using Bosch etching,[30] and channel heights of more than one millimetre have been fabricated using fused deposition modelling (FDM)[24,31] and stereolithography (SLA)[32] 3D printing techniques (Box 1). Plants such as *A. thaliana* form a relatively large primary root that grows from the seed, which then branches laterally. This root architecture is amenable to a singular straight microchannel design. However, some plants develop fibrous root systems (Fig. 1D), which consist of multiple thinner roots growing from the seed. This makes the singular straight microchannel design unsuitable. Chai *et al.* overcame this issue using a multichambered "petaloid" design (Fig. 1E and F), consisting of five separate chambers for root observation, and showed the utility of the petaloid root growth microfluidic (PRGM) device in growing *O. sativa* (rice).[24] In summary, microfluidic devices facilitate high resolution spatiotemporal imaging over long time periods through focal confinement of the plant root. Multiple microfabrication techniques have been employed for manufacturing microchannels of an appropriate size for focal confinement, which are dependent on the size and root architecture of the study species.

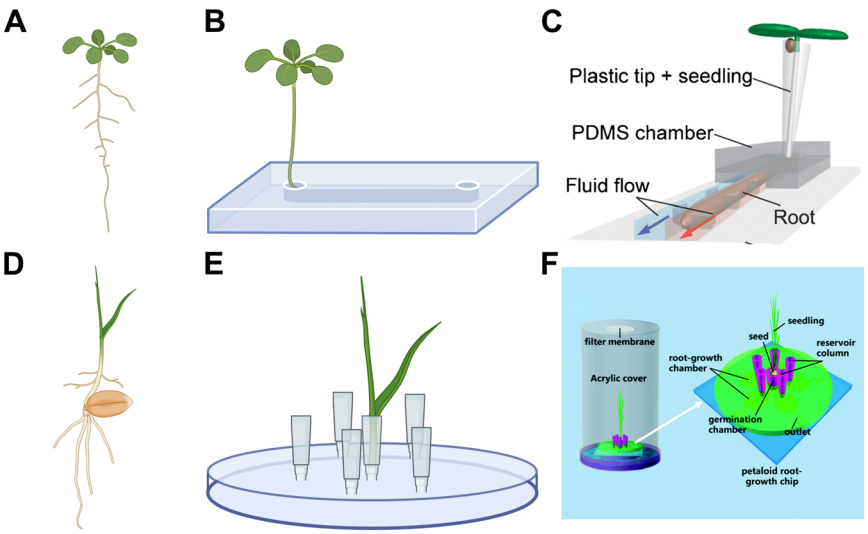

Fig. 1 Plants require different microfluidic device designs due to differences in root architecture. (A–C) Plants that form a single primary root during the seedling stage such as *A. thaliana* (A) can be accommodated in a single straight microchannel device design (B), such as the dual-flow-RootChip (C). (D–F) Plants that form multiple such as rice and wheat often form fibrous root systems (D), which require more complicated device designs to accommodate multiple roots (E), such as the petaloid root growth microfluidic (PRGM) chip with 5 chambers to confine each root individually (F). Image in (C) produced with modification from ref. 28 with permission from John Wiley and Sons, copyright 2023. Image in (F) produced with modifications from ref. 24 with permission from the Royal Society of Chemistry, copyright 2018. Created in BioRender. Cohen, L. (2025) https://BioRender.com/hgd4y66.

Box 1

The microfabrication of microfluidic devices can be achieved through a variety of techniques. Photolithography is used to fabricate microfluidic devices with small feature sizes (microchannels, microchambers, *etc.*). Photolithography involves first spinning a photoresist onto a silicon wafer at a controlled thickness, determining the height of the structures. Subsequently, ultra-violet (UV) light is applied through a photomask to write structures onto the photoresist, determining the length and width of the structures. These patterned silicon wafers form the negative "master mould" of the microfluidic device. Photolithography reliably achieves feature size resolution as small as 1 μm and layer heights as small as 2 μm but typically requires access to specialised equipment and training. Moreover, the maximum height of structures produced by spin coating a single layer of commercially available photoresist is around 200 μm. While this channel height is suitable for *A. thaliana* primary roots, it is unsuitable for larger root systems. While it is possible to modify the photolithography process to produce thicker structures by replacing photoresist spin coating with constant volume injection,[33] this has not yet been attempted for manufacturing large straight channels for roots, and layer heights have more variation than when spin coating. Therefore, alternative microfabrication technologies are required for large microchannel structures. 3D printing technologies have decreased in cost and increased in resolution over the past two decades, making them a viable alternative to photolithography for producing large channel designs (reviewed by Su *et al.*).[34]

Fused deposition modelling (FDM) 3D printing involves melting a thermoplastic filament and depositing sequentially in layers to form a final master mould product. FDM 3D printing technologies have come down in cost drastically over the past two decades and are straightforward to use. Device designs can be iterated on very quickly, and the material cost of printing designs is low. However, FDM 3D printers are limited to minimum layer heights of several hundred micrometres, with minimum feature resolutions of 50 μm, making them unsuitable to fabricate the smaller layer heights needed for root hair, and protoplast trapping interaction studies. Moreover, issues with surface roughness (which are translated to the PDMS device) are an issue for achieving high-resolution imaging. Therefore, FDM 3D printing is a useful microfabrication technique for microfluidic device designs with simple, large microchamber geometries.

Stereolithography (SLA) 3D printing involves using a light source to cure liquid resin into solid objects layer by layer. SLA printing can achieve feature resolutions of up to 10 μm (though this varies greatly depending on printer model) and offers a middle ground of resolution, price, and iterative speed, between FDM 3D printing and photolithography. SLA 3D printing technology can theoretically achieve layer heights as low as 15 μm, meaning it could be used for both small and large layer heights, making it amenable for root hair and protoplast trapping interaction studies. Initial surface roughness of the master mould can be post-processed to achieve low surface roughness. Hence, SLA 3D printing has been used for the manufacture of microfluidic devices used for root–chemical interactions[32] and plant phenotyping[35] (Fig. 13). By combining SLA 3D printing technology with transparent biocompatible resins, microfluidic devices can be manufactured directly, instead of producing a negative master mould and using PDMS. This makes scalable manufacturing of microfluidic devices possible, in use cases where many microfluidic devices are needed. As the cost of advanced SLA 3D printing technology continues to fall, and resolution continues to increase, this technology may rival the capabilities of photolithography and decrease the barrier to entry for microfluidic device manufacturing.

Comparison of technologies for microfluidic device fabrication.

	Photolithography	FDM 3D printing	SLA 3D printing
Maximum structure height	200 μm (single spin coat)	>100 mm	>100 mm
Minimum structure height	2 μm	>100 μm	15 μm
Resolution	1 μm	>50 μm	10 μm
Surface roughness	Smooth	Rough	Smooth (with modifications)
Cost and expertise	High	Low	Medium–high

2.2 Microfluidic device-assisted imaging of root–chemical interactions

Temporal manipulation of chemical microenvironments. In classical agar-based approaches, temporal manipulation of the chemical environment is achieved by manually moving plants between agar plates containing different chemical treatments, resulting in handling-related stress responses, and large (minutes to hours) time intervals between treatments. Since microfluidic microchannels are filled with liquid media, syringe pumps can be used to manipulate the fluidic environment surrounding plant roots. Chemical treatments can be applied by changing the media that syringe pumps feed into the microfluidic device, which reduces the problem of nutrient depletion zones around the root, and allows chemical treatments to be changed quickly with minimal root handling. While changing media conditions on agar plates can take a significant amount of time if a large sample size of plants is needed, microfluidic technology facilitates changing media within a matter of minutes to seconds for large sample sizes, depending on the technique used. These advantages have been leveraged to gain new insights into the temporal relationship of root–chemical interactions. For example, Moussus and Meier grew *A. thaliana* seedlings first in Murashige–Skoog media and then changed to polyethylene glycol (PEG, a chemical that results in osmotic stress)-spiked media of varying concentrations without needing to handle the root.[32] The authors found that higher concentrations of PEG (and therefore higher osmotic stress) resulted in stunted and abnormally shaped roots with a higher density of root hairs.[32] Because the internal environment of microfluidic devices is controlled using syringe pumps, chemical treatments can be changed quickly in less than two minutes without handling the root. Microfluidic devices have also facilitated faster (*i.e.*, less than one minute) exchange of different media

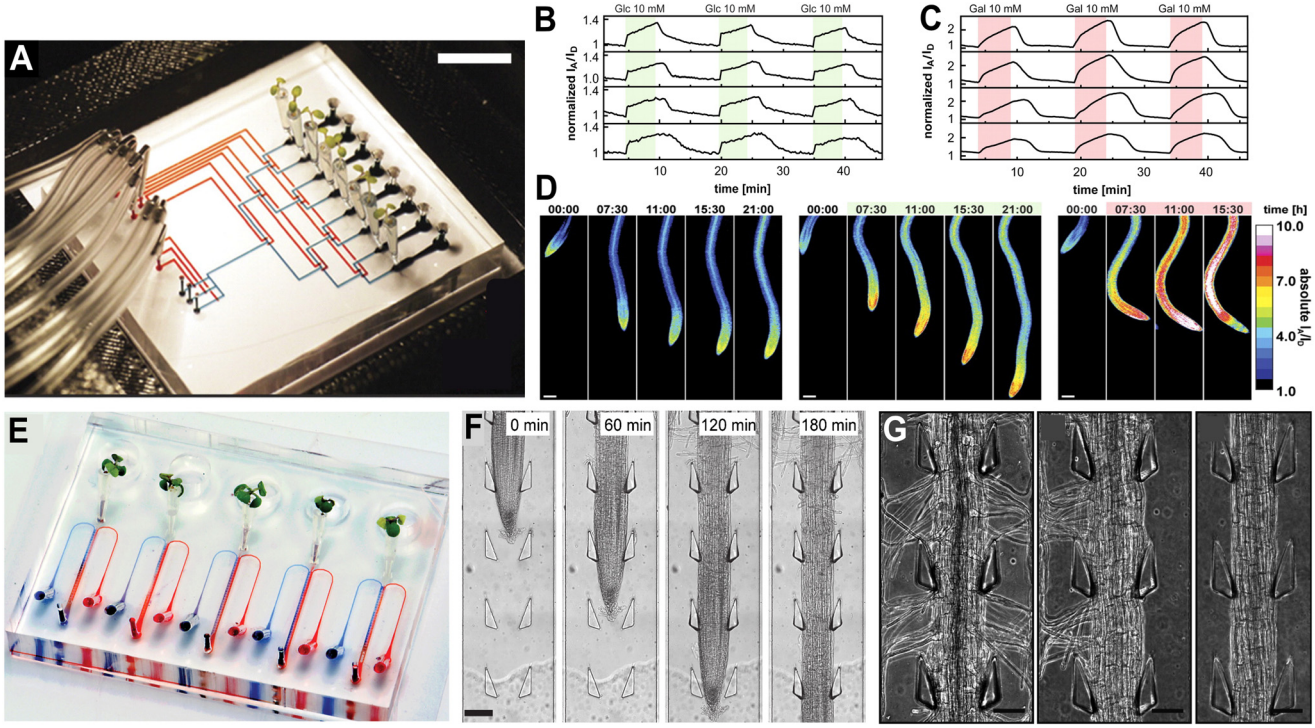

Fig. 2 The RootChip and dual-flow-RootChip facilitate studies on root–chemical interactions. (A) The RootChip can accommodate eight mounted live *A. thaliana* plants, with eight control (blue) and flow (red) channels filled for illustration. Bar = 1 cm. (B and C) The RootChip was used to monitor intracellular glucose (B) and galactose (C) concentrations over time using a FRET biosensor. When exogenous glucose and galactose was applied, an initial increase and subsequent levelling off of both intracellular glucose and galactose concentrations was found, suggesting the presence of a uniport mechanism for hexoses. (D) The FRET intensity ratios of roots growing under the control (left), glucose (middle), and galactose (right) conditions over time was investigated. Images produced with modification from ref. 22 under a Creative Commons Attribution License CC-BY 4.0 (https://www.creativecommons.org/licenses/by/4.0/). (E) The dual-flow-RootChip can accommodate five mounted live *A. thaliana* plants. Two inlet channels serve each chamber, and red and blue dyes illustrate how two different reagents can be applied simultaneously to either side of the root. (F) *A. thaliana* roots are guided by PDMS support pillars. (G) Under symmetric osmotic stress conditions, where the medium contains 20% (w/v) PEG 8000 on both sides (right panel), no root hairs are observed. Under asymmetric osmotic stress conditions, with 20% (w/v) PEG 8000 applied only to the right side of the root (middle panel), root hairs are absent on the PEG-exposed side. In contrast, roots grown without PEG 8000 (left panel) show normal root hair development. Images produced with modification from ref. 28 with permission from RSC publishing, copyright 2018.

treatments to monitor very fast developmental responses. For example, by integrating pressure-actuated microvalves (Quake valves) into the RootChip, RootChip-16, and later the vertical RootChip (vRootChip), short bursts of chemical treatment were able to be applied to the root.[22,36,37] In the vRootChip, Fendrych *et al.* changed the flow direction and mounted the vRootChip vertically.[37] They were able to show that the growth rate of *A. thaliana* roots rapidly reduced (within 30 seconds) or recovered (within 2 minutes) when auxin was present or absent, respectively. The authors suggested that because this response was faster than transcription and translation of auxin-induced genes, this part of the auxin response must be regulated through non-transcriptional means. In summary, microfluidic technology facilitates the temporal manipulation of the chemical environment by quickly exchanging chemical treatments inside microfluidic channels. This can be achieved using syringe pumps and through pressure-actuated microvalves, depending on the timescales of the developmental response being investigated.

Spatial manipulation of chemical microenvironments. Microfluidic technology can facilitate spatial manipulation of the chemical environment using laminar flow to localise a chemical treatment to a root section instead of the entire root, as the treatment and control media remain spatially separated inside the microfluidic device. For example, Meier *et al.* used a series of laminar flow perfusion channels perpendicular to the primary root channel to control the area of the root treated with synthetic auxin.[13] The authors showed that localised stimulation of the root apex using synthetic auxin resulted in outgrowth of root hairs from the stimulated region of the root confined within the device. Therefore, Meier *et al.* utilised laminar flow to manipulate the chemical microenvironment along the proximal/distal axis of the root.[13] On the other hand, Stanley *et al.* exploited laminar flow in the dual-flow-RootChip (df-RootChip, Fig. 2) to manipulate the chemical environment along the lateral (left/right) root axis, perfusing two different chemical treatments on either side of the same *A. thaliana* primary root.[28] The authors show a spatially explicit osmotic stress

response by exposing PEG-enriched media to one side of the root. Moreover, asymmetric stimulation of phosphate deficiency was shown to result in asymmetric changes in root hair phenotype (root hair length) and gene expression (expression of the root hair transcriptional regulator RSL4). Subsequently, the df-RootChip was modified; first, by adding extra inlets to allow independent stimulation on either side of the root in the bi-directional-RootChip (bi-df-RootChip),[38] and then by connecting the bi-df-RootChip to a multiplexed media delivery system (MMDS). This was found to increase the spatial resolution at which chemical gradients can be generated inside the bi-df-RootChip.[39]

Investigating root–chemical interactions of plants with fibrous root systems requires multiple root chambers to separate individual roots of fibrous root systems. In this instance, spatial manipulation of the chemical microenvironment can be achieved by differentially treating individual roots of the same root system. Chai *et al.* chemically treated individual roots of the fibrous root system of *O. sativa* with a range of concentrations of PEG.[24] The authors showed that exposure to PEG in higher concentrations was correlated with roots showing delayed growth, and an increase in root hair density. In summary, manipulation of the chemical microenvironment can be achieved at different spatial scales – at the scale of a single root by separating which area of a single primary root is treated (proximal/distal, left–right axis), as well as at the scale of a root system by treating different roots of the same fibrous root system to different chemical treatments.

Genetically encoded biosensors and microfluidic technology. We have seen how combining high-resolution imaging and manipulation of chemical microenvironments has yielded valuable biological insights into root–chemical interactions using microfluidic technology. Further insights can be made using genetically encoded biosensors, and down-stream chemical analysis of fluid and plant tissue extracted from microfluidic devices. Genetically encoded biosensors allow for non-invasive real-time analysis of metabolite fluxes in living tissues of genetically modified plants.[21] Combined with high resolution spatiotemporal imaging, root–chemical responses can be linked to specific cellular machinery, opening the door to understanding the genetic mechanisms for phenotypic responses. For example, Grossmann *et al.* used *A. thaliana* plants transformed with glucose and galactose Förster resonance energy transfer (FRET) biosensors in the RootChip to quantify intracellular glucose and galactose concentrations (Fig. 2A–D). The authors used FRET biosensor intensity ratios data to track where glucose and galactose are localised within the root, as well as their relative concentrations, over time.[22] This data allowed the authors to analyse the dynamics of changes in intracellular glucose and galactose concentrations when subject to 10 mM pulses in exogenous glucose and galactose respectively. An initial increase and subsequent levelling off of both intracellular glucose and galactose concentrations was found (Fig. 2B and C), suggesting the presence of uniport mechanisms for hexoses transport. Continuing this approach, Lanquar *et al.* used zinc FRET sensors in the RootChip to untangle dynamics between zinc stores and free zinc in different zinc availability environments.[27] The authors estimated concentrations of cytosolic free zinc in *A. thaliana* seedlings grown in sufficient and excess zinc supply channels. Their results suggest that root cells have a high-affinity zinc uptake mechanism, allowing efficient uptake of zinc in the 100 nM range. The genetically encoded calcium indicator (GECI) R-GECO1 has been leveraged to observe calcium dynamics in living root tissue first by Keinath *et al.* using the RootChip16.[36,40] By leveraging high-resolution imaging offered by microfluidic technology, authors were able to use R-GECO1 to measure calcium oscillations in individual root hair cells.[41] Finally, Stanley *et al.* used the biosensor R-GECO1 to image cytosolic calcium in *A. thaliana* root cells to observe the plant immune response upon exposure to flg22.[28] In summary, genetically encoded biosensors sensors complement the benefits of high-resolution imaging and chemical manipulation of the microenvironment offered by microfluidic technology. This facilitates studies on subcellular nutrient dynamics and immune responses in plant roots.

Chemical assays and microfluidic technology. Microfluidic devices are designed for effective optical, but not chemical, interfaces with the internal microenvironment. This means methods for chemical analysis such as targeted staining, mass spectrometry, and qPCR cannot easily be combined with microfluidic technology, limiting its utility. Two approaches have been shown in the literature to date to overcome this limitation in root–chemical interaction studies: i) devices can be designed to be openable for material extraction while retaining glass coverslips as the optical interface material and ii) selectively permeable chemical membranes can replace chemically impermeable glass coverslips as the device interface material for assay-specific chemical access of the internal device environment. It is not usually possible to disassemble microfluidic devices, partly because device fabrication typically involves a PDMS slab embossed with microchannels and/or microchambers being bound covalently to a glass (or PDMS-coated) coverslip using plasma treatment. This makes extracting fluid for further analysis impractical, as fluid must be collected at device outlets, meaning spatial data of where the fluid came from inside the microfluidic device is lost. Moreover, extracting plant tissue for further analysis is not possible without breaking the device, resulting in the loss of fine spatial data, and potential contamination of the sample. Chai *et al.* approached this problem by mechanically clamping (instead of chemically bonding) PDMS to glass coverslips, making it possible to open and reseal the Lid open-seal Switchable Plant Chip (LSPC) device. This allowed the authors to remove root sections and media for further analysis.[42] The authors show the utility of this device by extracting root sections and measuring reactive oxygen species (ROS) using the

fluorescent dye 2′-7′dichlorofluorescin diacetate (DCFH-DA), performing quantitative real-time PCR for expression of osmotic stress response-related genes, and measuring the concentration of soluble sugar.

Aufrecht *et al.* took a different approach and designed the rhizosphere-on-a-chip microfluidic device to interface with liquid micro-junction surface sampling mass spectrometry (LMJ-SSP-MS) (Fig. 4).[30] The authors achieved this by replacing the glass coverslip interface material with a polyester track-etched (PETE) membrane. This transparent membrane has a high density of 0.4 μm diameter pores, facilitating transport of small molecules such as amino acids from root exudates through the membrane for quantification, while preventing fluid leakage. The properties of this PETE membrane were leveraged to allow both an optical and chemical interface with the device, meaning the authors were able to image root growth at cellular resolution, as well as map the relationship between amino acid concentrations and artificial soil pore geometry at a coarser spatial scale. This membrane interface approach has the potential to provide both optical and chemical interfaces with the device but does not allow for plant tissue to be extracted, limiting analysis to specific analytical techniques compatible with membrane-interface sampling. Further development of both openable and membrane interface microfluidic devices is of great interest to the field of plant microfluidics. In summary, microfluidic devices can be designed to be amenable to analytical techniques to yield further insights into root–chemical interactions. Modifying microfluidic devices to enable compatibility with analytical techniques results in imaging trade-offs but has the potential to facilitate a broader range of data collection from microfluidic systems.

2.3 Microfluidic device-assisted imaging of root–microbe interactions

We have seen how microfluidic technology has contributed to an improved understanding of how plant roots respond to dynamic and spatially heterogeneous chemical environments. Biotic environments are another important factor contributing to rhizospheric heterogeneity and dynamism. Soil microbes interact with plant roots in pathogenic, commensal and mutualistic relationships, and have major impacts on plant health and ecosystem productivity.[43] Classical plate, hydroponic, and pot-based assays for root–microbe interaction studies provide valuable insights into how microbes can alter plant phenotypes at coarse spatial scales, but understanding these interactions at a cellular level is difficult using classical techniques. Observing root–microbe interactions with cellular resolution allows the investigation of how microbes search space, forage for nutrients and disperse in rhizospheric environments. Microfluidic technology offers a way to construct a simplified rhizospheric ecosystem and facilitates high-resolution imaging of soil microbes, as well as their impact on plant roots. Observations of growth and space-searching behaviours of plant roots and soil microbes can be combined with fluorescently labelled microbes to characterise spatiotemporal variation in these interactions. Microfluidic devices used to investigate root–microbe interactions use single layer microchannel designs similar to devices used to investigate root–chemical interactions (Section 2.2). These microchannels facilitate focal confinement of the root, but not the smaller microbial partner, within the comparatively large plant root microchannel. Therefore, the growth and space-searching behaviour of the microbial partner cannot easily be observed in real time. However, biological inferences can be made using: i) observation of the impact of the microbial partner on root morphology, and ii) direct observation of the microbial partner using fluorescent microbes or image processing techniques.

Observation of microbial impacts on root morphology. The first microfluidic devices for studying root–microbe interactions were limited in that focal confinement of the microbial partner within the primary root microchannel was poor. For example, Parashar and Pandey grew *A. thaliana* seedlings inside the Plant-in-Chip device, and subsequently inoculated *Phytophthora sojae* zoospores, as well as sugarbeet nematodes, through perpendicular inoculation channels.[44] The authors were able to observe appressoria formation and darkened root cells, possibly indicating root cell death, upon *P. sojae* zoospore inoculation. Due to their larger size, sugarbeet nematodes were observed directly navigating towards the root and establishing feedings sites. Similarly, Jiang *et al.* introduced *P. sojae* zoospores into a microfluidic device designed for high-throughput phenotyping of *A. thaliana* seedlings without modifying the device design.[26] The authors were able to achieve this through hydrodynamic loading of *A. thaliana* seeds, allowing further inoculation with spores to take place after seed inoculation. The authors observed brown spots on *A. thaliana* seedlings due to localised cell death after 50 h.

Observing spatial root–microbe interactions. Insufficient focal confinement of the microbial partner can be supplemented with fluorescently labelling the microbial partner, or through computational image analysis to directly observe the microbial partner. This facilitates higher resolution spatial data to be obtained while keeping the same device design as devices used for root–chemical interactions. For example, Massalha *et al.* developed the tracking root interaction system (TRIS) device, which combines a single channel device geometry for *A. thaliana* seedlings with two fluorescently labelled bacterial strains (*Bacillus subtilis* and *Escherichia coli*) (Fig. 3).[45] The authors were able to use the contrasting fluorescent signals from either bacterial strain to assess the spatial distribution of the two bacterial strains throughout the root over time. Firstly, the authors observed rapid chemotaxis of *B. subtilis* towards the elongation zone of the growing *A. thaliana* root. *B. subtilis* chemosensing knockout mutants were found to

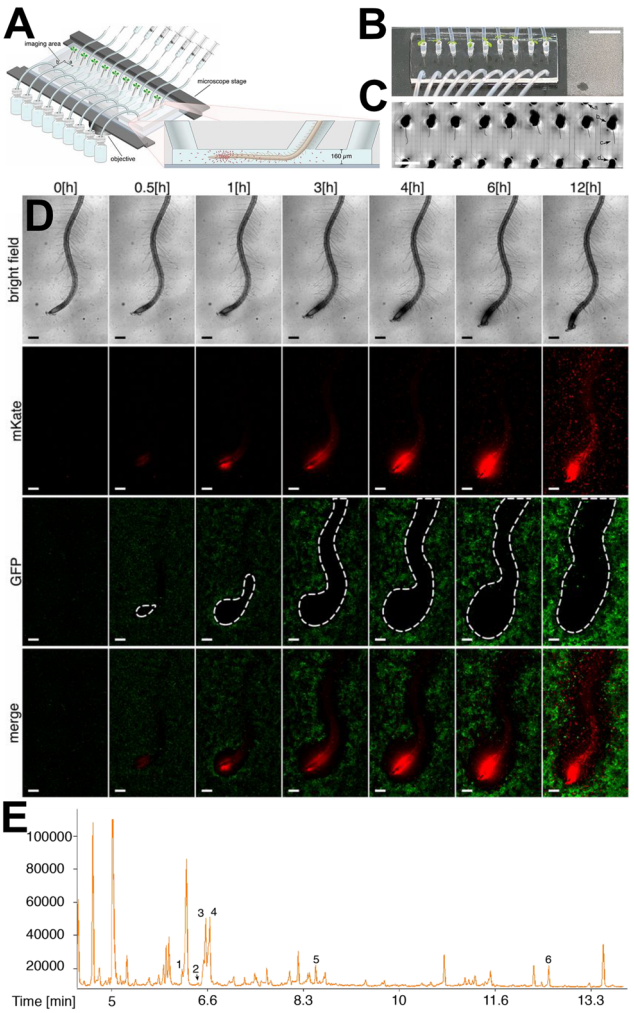

Fig. 3 The Tracking Root Interaction System (TRIS) microfluidic device facilitates spatial root-bacterial interactions. (A) Schematic illustration of the TRIS device mounted on a microscope mount, including a side view of a single microfluidic root channel containing root and bacterial cells (insert, not to scale). (B) Top view of *Arabidopsis thaliana* plants growing inside plastic pipettes attached to the TRIS device. Scale bar, 1 cm. (C) Micrograph of nine *A. thaliana* roots growing inside the TRIS device captured with 10× magnification brightfield. Arrows: a, inlet port; b, tip inside a root-dedicated port with c, a root extending towards the outlet port; d, outlet port. Scale bar, 5 mm. (D) Select micrographs from four independent imaging experiments showing bacterial competition for the root surface. Wild-type (WT) *A. thaliana* (brightfield channel) was incubated with GFP-labelled *Escherichia coli* (green) and mKate-labelled *Bacillus subtilis* (red). White dashed area in GFP images indicate the exclusion zone of *E. coli* bacteria from the root by *B. subtilis*. Scale bars, 200 μm. (E) The TRIS device also facilitates single-root exudate metabolomics. Selected ion chromatogram showing a representative metabolite profile from a single-root exudate of a 10-day-old WT *A. thaliana* root grown in the TRIS device, analysed with gas chromatography coupled to time-of-flight mass spectrometry. The numbered peaks correspond to selected metabolites identified from authentic standards: (1) phosphoric acid, (2) isoleucine, (3) glycine, (4) succinic acid, (5) pyroglutamic acid, and (6) myo-inositol. Images produced with modification from ref. 45 with permission from Proceedings of the National Academy of Sciences of the United States of America, copyright 2017.

show a reduction in attraction, suggesting a role of root exudate sensing in chemoattraction. Secondly, the authors observed an exclusion zone of *E. coli* by *B. subtilis* of up to 100 μm from the root (Fig. 3D), suggesting a diffusible signal from *B. subtilis* or the root, causing *E. coli* exclusion. Lastly, single root exudate metabolite profiling was performed by collecting media and analysing using gas chromatography coupled to time-of-flight mass spectrometry (Fig. 3E). Therefore, fluorescently labelled microbial partners allows the spatiotemporal dynamics of root–microbe interactions to be investigated. In another study looking at bacterial colonisation of *Populus tremuloides* (aspen) seedlings using the root–microbe interaction (RMI) chip, fluorescently labelled *Pseudomonas fluorescens* bacteria were shown to colonise *P. tremuloides* with dynamic biofilm formation in a similar manner to what has been reported in other experimental setups.[23] Moreover, the authors attempted to use whole-cell biosensors in the form of transformed *B. subtilis* strains to observe dynamic changes in extracellular xylose and reactive oxygen species (ROS). However, the authors found that these biosensor strains did not adhere to the root surface well and were instead mostly washed off with media flow, in contrast to *P. fluorescens*. This shows the importance of designing biosensor bacterial strains using naturally colonising bacteria, and displays the tradeoff between realistic model interaction systems, and the availability of genetic toolkits. Lastly, Conway *et al.* took a similar approach in designing the Arabidopsis Root Microbiome Microfluidic (ARMM) device, which has a larger microchamber to accommodate older *A. thaliana* plants, and imaged spatial patterns of root-bacterial interactions using a fluorescently labelled *Pseudomonas* strain.[46]

In microbial partners where fluorescent labelling is more difficult, computational approaches can be used to improve the visualisation of the microbial partner in rhizospheric environments. Cohen *et al.* used software to track the movement of motile *Phytophthora parasitica* zoospores as they approached an *A. thaliana* root from the device outlet.[47] The authors were able to show that compared to a non-root control, the presence of the root alters the speed distribution of zoospores, and that the movement speed and directedness of zoospores is only impacted at a distance of 300 μm or less from the root, suggesting a root-derived signal diffusible over short distances. Therefore, fluorescent labelling, whole-cell biosensors, and computational image processing are useful tools for investigating microbes in a large root channel to compensate for insufficient focal confinement.

2.4 Microfluidic device-assisted imaging of root–physical interactions

We have seen how microfluidic technology can uncover spatial interactions between roots and chemical agents, as well as roots and soil microbes, but just as important for understanding root–rhizosphere dynamics is the interplay between roots and the physical structure of the soil around

them. Plant roots are influenced by and reshape the physical structure of soil, which impacts soil properties such as nutrient hotspots,[48] contributing to the complexity of soil across a continuum of spatial scales. For example, it has been observed that bacterial strains that cannot coexist in a spatially homogeneous environment can coexist in a spatially heterogeneous environment.[49] How the physical structure of soil generates these niches is a subject of great interest for soil scientists, but simplifying the soil system to investigate individual hypotheses is difficult. Microfluidic technology is uniquely suited to investigate this interplay as the complex structure of soil can be simplified to investigate individual hypotheses and therefore reduce the complexity of experiments. For example, Aufrecht *et al.* set out to investigate the impact of soil particle shape and size using the rhizosphere-on-a-chip device (Fig. 4).[30] The authors constructed a natural sand-mimicking particle structure and introduced the model grass *B. distachyon* into this microchamber. The authors showed that this spatial heterogeneity resulted in hotpots of amino acid root exudates in comparison to an open geometry control, as measured using LMJ-SSP-MS, and profiled the variability in amino acids detected at several sampling sites (Fig. 4C). The growth of roots and root hairs into small interpore spaces (Fig. 4B) was observed alongside amino acid exudate data. A subsequent study using the same device but using *Cannabis sativa* (hemp) as the model organism, showed the utility of rhizosphere-on-a-chip devices for studying a range of plants with larger root systems.[31]

Microfluidic technology can also be utilised to investigate growth behaviour mechanics and quantify physical properties of plant. For example, Zhang *et al.* observed the impact of channel width and sharp corners on the rate of root growth in *A. thaliana*.[50] Liu *et al.* used sodium chloride as an osmotic treatment to measure cell wall elasticity using the RootChip-8S.[51] By applying media flow to growing *A. thaliana* roots, Agarwal *et al.* were able to induce and monitor thigmomorphogenesis inside a custom microfluidic device.[52] Li *et al.* utilised a custom microfluidic device with a cantilevered sensing pillar to measure the protrusive force of a growing *A. thaliana* root.[53] Lastly, intracellular dynamics upon root compression was monitored using a custom microfluidic device that applies mechanical stimulation to a growing *A. thaliana* root. Vinet *et al.* used a two-chamber microfluidic device design, with the top chamber exerting a compressive force on a growing *A. thaliana* root in the lower chamber. The authors were able to monitor changes in ROS and intracellular calcium using probes and GECIs respectively.[54] In summary, microfluidic technology has recently given important insights into how roots interact with the physical structure of soil to create a spatially heterogeneous environment, but there are still many open questions. For example, integrating studies of physical structure with soil microbes, and looking at how physical structures generate unique chemical microenvironments, which in turn create biological niches for microbial colonisation.

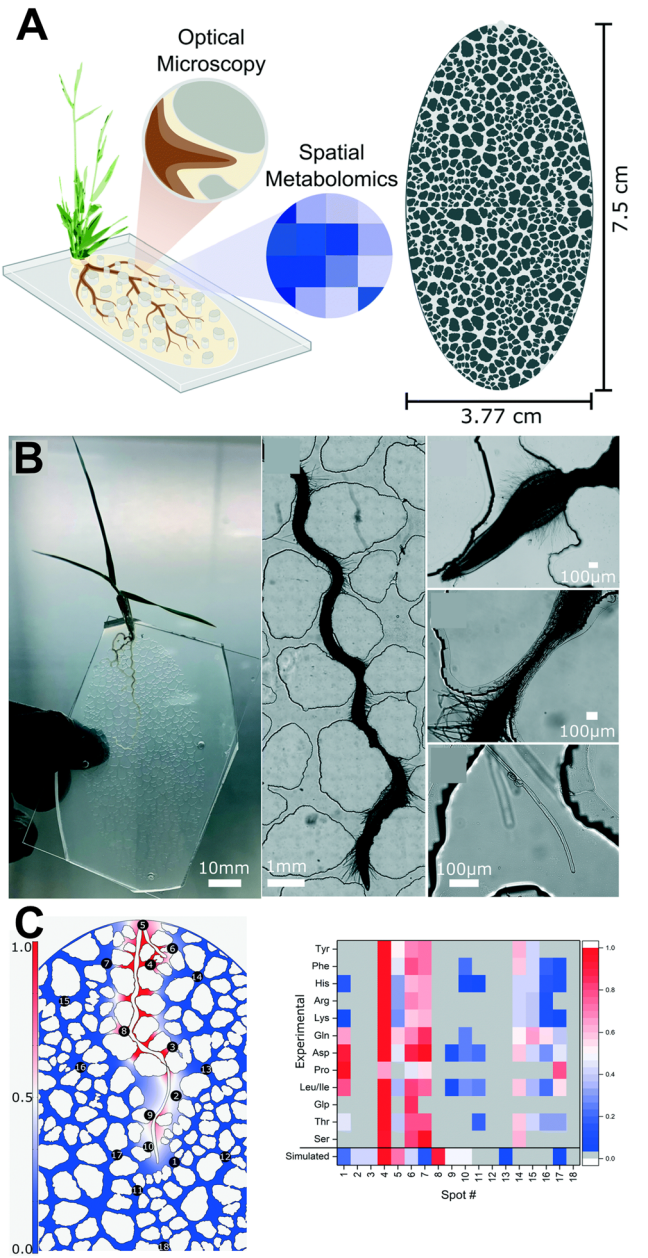

Fig. 4 The rhizosphere-on-a-chip facilitates root–physical interaction studies. (A) The rhizosphere-on-a-chip mimics the pore structure of natural sands, and allows both optical microscopy and spatial metabolomics of the root's microenvironment through liquid micro-junction surface sampling mass spectrometry (LMJ-SSP-MS). (B) The rhizosphere-on-a-chip allows long-term culturing of *Brachypodium distachyon* roots (from left right); a seedling reaches developmental milestones two weeks post germination, roots are able to navigate small spaces, root hairs span inter-grain gaps. (C) Amino acid exudate hotposts are detected and spatially resolved within the microchannels. The left panel shows simulated root exudate concentrations after two hours of flux from the traced root boundaries of a biological replicate. Numbered circles represent spots where root exudates were sampled using LMJ-SSP-MS. The right panel shows a heat map comparing the amino acid profiles of simulated and experimental replicates from each spot sampled from a 12-day old *B. distachyon* root. Images produced with modification from ref. 30 under a Creative Commons Attribution License CC-BY 3.0 (https://creativecommons.org/licenses/by/3.0/).

3 Microfluidic device-assisted imaging of tip-growing plant cells

Tip-growing plant cells are an evolutionarily diverse group of plant cells, which share an ancestral mechanism of lateral extension. Unlike plant roots, which grow by meristematic division, tip-growing plant cells use turgor pressure and cell wall remodelling to expand and grow forwards.[55] Three different types of tip-growing plant cells will be discussed: pollen tubes (tubular protrusions formed by the pollen grain of flowering plants in the angiosperm clade), moss protonemata (filamentous networks formed from haploid spores by mosses in the bryophyte clade), and root hairs (terminally differentiated lateral extensions of root epidermal cells (trichoblasts) and are formed by almost all land plants). Tip-growing plant cells are single cells, meaning their growth rate, direction, intracellular processes, and branching behaviour (where applicable) must be investigated at single-cell resolution. This makes tip-growing plant cells difficult to study in classical plate-based approaches due to insufficient focal confinement, and therefore the optical advantages afforded by microfluidic technology are particularly useful in studying tip-growing plant cells. As a result, the development of microfluidic technology for studying tip-growing plant cells has been an important research focus in the field of plant microfluidics over the past two decades. While these three types of tip-growing plant cells are morphologically and evolutionarily diverse, their shared method of growth means designing microfluidic devices to study their growth and development shares a common approach, with slight differences in device design depending on the biological question being asked. For example, a common device consideration is how to focally confine tip-growing plant cells. In pollen tubes and moss protonemata, this means specialised structures to trap pollen grains[56] and moss spores or protoplasts, respectively.[57] Whereas in root hairs, this takes the form of a multilayer device fabrication process, with separate layers to focally confine the root and root hairs.[58]

3.1 Microfluidic device-assisted studies on pollen tubes

Pollen tubes are tubular protrusions formed by the pollen grain when landing on a receptive stigma and deliver male gametes from the pollen grain to the female gametophyte in the flower ovule. The speed of pollen tube elongation directly influences fertilisation success, and therefore is strongly selected upon, resulting in pollen tube elongation rates up to 600 μm h^{-1}.[59] Pollen tube growth can be triggered *in vitro* with virtually identical morphology to *in vivo*,[60] albeit with slower growth rates. The pollen tube must invade plant tissue inside the pistil of the receptive flower[61] and grow through gaps between cells smaller than the diameter of the pollen tube.[61,62] Though it is likely some digestive action by enzymes and programmed cell death of the pistil tissue facilitates pollen tube growth, it is unlikely that the substrate is liquefied completely.[63] Therefore, the pollen tube likely exerts a penetrative force and must search space and navigate challenging environments using chemical, physical, and possibly electrical, cues. Microfluidic technology is a useful way to study pollen tube guidance as it allows high-resolution imaging of growing pollen tubes and can be designed to mimic the environment pollen tubes are exposed to *in vivo*.

Microfluidic device-assisted imaging of pollen tube growth dynamics. Characterising the growth dynamics of pollen tubes at single-cell resolution under controlled conditions is of great interest to plant scientists, as it gives insights into the mechanisms behind pollen tube growth, and how pollen tubes behave *in vivo*. Agudelo *et al.* developed the TipChip device, which facilitates the observation of *Camellia japonica* pollen tubes navigating through challenging microchannels mimicking the spatial complexity of an ovule.[64] The authors showed that pollen tubes follow the direction of growth of microchannels regardless of microchannel shape, exemplifying the ability of *C. japonica* pollen tubes to navigate challenging environments mimicking an ovule. Building on this work, the authors showed that, unlike fungal hyphae and root hairs, pollen tubes do not have directional memory.[65] The TipChip was successful in showing the growth dynamics of individual pollen tubes in custom microchannels and successfully revealed novel aspects of pollen tube growth dynamics but had several issues. Firstly, due to imprecise pollen grain loading, multiple pollen grains often became trapped in the same microchannel. This results in multiple pollen tubes growing into the same microchannel, blocking the channel and therefore altering the flow characteristics. This means that the *in vitro* conditions of each pollen tube are not precisely controlled, which could result in different growth dynamics, making individual replicates less comparable. To solve this, Ghanbari *et al.* developed a device specifically designed to trap a single pollen grain per channel.[56,66] The authors were able to achieve this by iterating on the TipChip device design with the most stable flow characteristics using COMSOL Multiphysics flow modelling.[67] The authors were able to achieve a single pollen grain trapped in each microchannel, at the expense of longer loading times. This device design was shown to be successful at exposing many replicates of pollen tubes to identical flow regimes and could be applied to other propagule structures such as fungal spores. The impact of physical obstacles on pollen tube growth was investigated further by Yanagisawa *et al.*, who investigated the ability of pollen tubes to penetrate gaps smaller than the diameter of their cells by constructing microchannels with different sized constrictions of microchannels.[68] The authors found that *Torenia fournieri* pollen tubes were able to deform their apical shape to grow through 1 μm microchannel constrictions, despite their cell diameter being 15–20 μm. However, when the gap length was extended, the pollen tubes were not able to grow through. This shows that there is a limit on the deformability of pollen tube cell walls and suggests that short instead of long narrow constrictions may be an obstacle present in ovules.

Microfluidic device-assisted imaging of chemosensing in pollen tubes. The chemosensing and electrosensing abilities of pollen tubes is of great evolutionary importance as it underpins our understanding of the cellular mechanism of angiosperm fertilisation. The first article to show that it is possible to perform chemosensing guidance assays of *A. thaliana* pollen tubes towards ovules used a simple microfluidic device design,[69] consisting of two perpendicular microchannels, one containing the pollen tubes, and one containing fertilised or unfertilised ovules. The authors showed that fluorescently tagged pollen tubes preferentially enter microchambers containing unfertilised ovules compared to fertilised ovules, suggesting that pollen tubes can sense and respond to diffusible chemical signals emitted by ovules. This finding was repeated by Horade *et al.*, who used a T-shaped channel design to show that *T. fournieri* pollen tubes selectively grow towards ovules.[70] Moreover, the authors found that UV irradiation of ovules decreased their ability to attract pollen tube growth. One issue faced by Yetisen *et al.* was distinguishing random pollen tube growth from directional growth.[69] This is because without a relevant chemical gradient, pollen tubes will grow randomly, reducing the statistical power of chemotropic assays. Yanagisawa and Higashiyama overcame this issue by integrating a series of "microslits" into the device design, which pollen tubes had to grow through to get to the unfertilised ovules.[71] This prevented randomly growing pollen tubes from growing through the microslits and only allowed pollen tubes with directed growth to pass through, thus facilitating a higher confidence in the chemotropic behaviour of pollen tubes. This device design also permits differentiation of chemotropically responsive pollen tubes within a population, potentially assisting in mutant studies.

While these studies provided robust evidence for chemotropic growth on groups of pollen tubes, higher resolution spatial control of the chemical agent is required to investigate the chemotropic growth of single pollen tubes. This has been achieved through laminar flow, and through integrating microfluidic pumps. Nezhad *et al.* utilised laminar flow inside the pollen tube microchannel, allowing continuous exposure to two different chemical agents on either side of a *C. japonica* pollen tube[72] (Fig. 5), in a similar way to the df-RootChip[28] as seen previously (Fig. 2D–F). The utility of the device was demonstrated through two experiments. Firstly, asymmetric application of extracellular calcium resulted in the pollen tube navigating to an optimal calcium concentration, as opposed to navigating to one side or the other, as would be expected by a single molecular mechanism of chemotropism. This suggests multiple interacting regulatory mechanisms controlling calcium chemotropism. Secondly, the enzyme pectin methyl esterase, which acts to rigidify the pollen tube cell wall, was applied extracellularly on one side of the pollen tube. This resulted in the growth direction of the pollen tube to turn away from the agent, which supports existing hypotheses of the mechanism of directional growth in pollen tubes. Therefore, the separation of chemical agents either side of the pollen tube using laminar flow is a useful way to conduct targeted

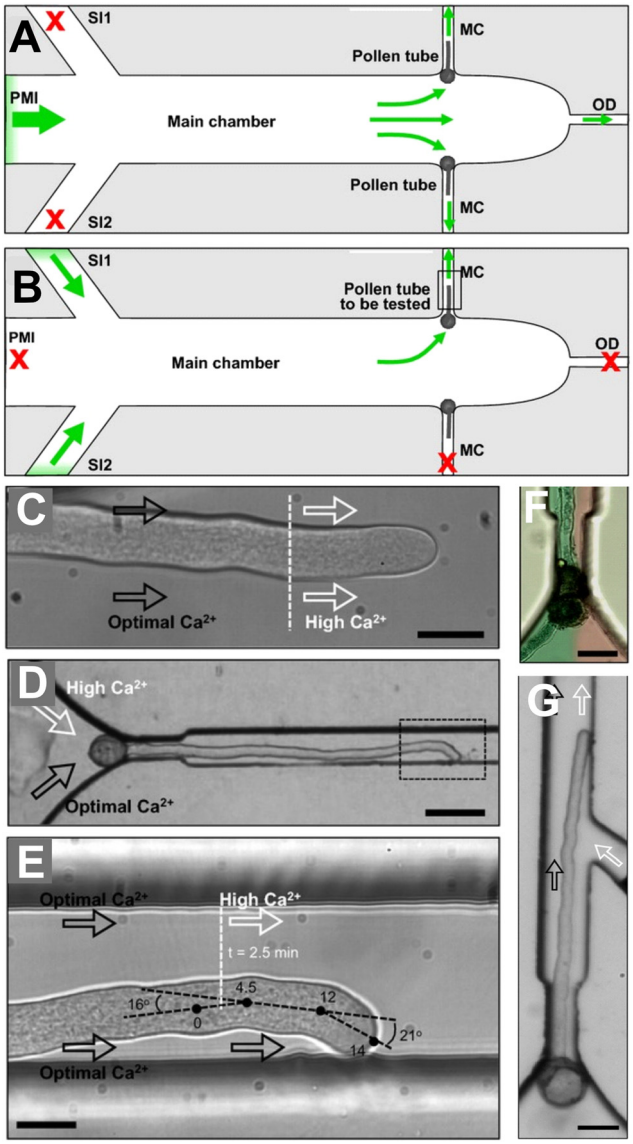

Fig. 5 Microfluidic device facilitates asymmetric application of calcium to growing *Camellia japonica* pollen tubes. (A) Pollen grains are first deposited and orientated correctly during experimental setup. (B) The pollen medium inlet (PMI) and one of the media channels (MC) are blocked during the experiment. Medium is injected through two side inlets (SI1, SI2). Drawings not to scale. (C) Pollen tubes were found not to change orientation during a global change from optimal calcium (2.54 mM) to high calcium (5.08 mM) but were found to slow down by 20%. Scale bar 20 μm. (D) Pollen tubes were found to reorientate when subject to asymmetric calcium. Scale bar, 70 μm. (E) Medium with optimal calcium concentration (2.54 mM) was supplied through both SIs, then high calcium (5.08 mM) was supplied through one of the SIs. The pollen tube was found to changes its growth rate and turn twice. Scale bar, 20 μm. (F) Asymmetric application of calcium was achieved through laminar flow, exemplified using red and green food colouring. Scale bar, 50 μm. (G) Alternative design where the channel delivers calcium only to the apical region of the pollen tube, not the base. Scale bar, 50 μm. Images produced with modification from ref. 72 with permission from John Wiley and Sons, copyright 2014.

chemotropic assays. On the other hand, Yanagisawa *et al.* achieved spatial control using a microfluidic injector device, which can inject a small volume of sample into the growth chamber utilising an on-chip electro-osmotic pump.[73] This allows for a small volume of reagent to be applied directly to growing *A. thaliana* pollen tubes. This technique offers an on-chip alternative to off-chip direct reagent application techniques, in which reagent is embedded onto a small bead, which in turn is placed on the growing pollen tube using a micromanipulator. This microfluidic injector device allows on-chip chemotropic assays without continuous flow, allowing chemotropic studies where flow is undesirable.

Microfluidic device-assisted imaging of electrosensing in pollen tubes. Chemosensing devices can be altered to investigate electrosensing in pollen tubes. Agudelo *et al.* designed a device to assay the impact of electrical charge on pollen tubes by altering the bottom glass coverslip of the device to contain a region with two microelectrodes on either side (Fig. 6).[74] This generates an electric field within a region of the device, and the impact of this electric field can be quantified optically. The authors showed differential effects of direct current (DC) and alternating current (AC) on pollen tube growth. Direct current electric fields caused pollen tubes to burst and growth rates to decrease, but alternating current fields were able to restore pollen tube growth rates. No directional effect was found on pollen tube guidance. Using a similar microfluidic device with microelectrodes, Hu *et al.* showed that DC currents only caused pollen tube bursting or arrest in growth when the tip overlapped the electrode, while bending away from the electrode occurred more often in other relative positions.[75] By measuring proton gradients, the authors pinpoint an inverse correlation between pH readings inside and outside the pollen tube and hypothesise excess proton pump activity as the cause of bursting. Agudelo *et al.* highlight a lack of consensus in studies on the effects of electric fields on plant growth and emphasise the importance of the ion content of media, and other factors that may contribute to conflicting results.[74] Hu *et al.* in particular mention electrolysis as a factor that can alter results.[75] Microfluidic technology is ideal for understanding pollen tubes' response to electrical stimuli because it allows for precise relative positioning of pollen tubes and electrodes, and the low fluid volumes required render Joule heating negligible.[76] However, this will need to be coupled with the use of inert electrode materials, such as platinum iridium, standardisation of the media and the electrode positioning used, as well as measurements of both electric field and current density.[77]

Microfluidic device-assisted imaging of mechanosensing in pollen tubes. The mechanosensing and exertion of force from pollen tubes is important in understanding how pollen tubes can penetrate into plant ovules. Mechanosensing is defined as a responsiveness to mechanical stimuli, especially at the cellular level. In plant cells, any pushing force is generated by the internal turgor pressure of the cell, as compared to being generated by the cytoskeleton in animal

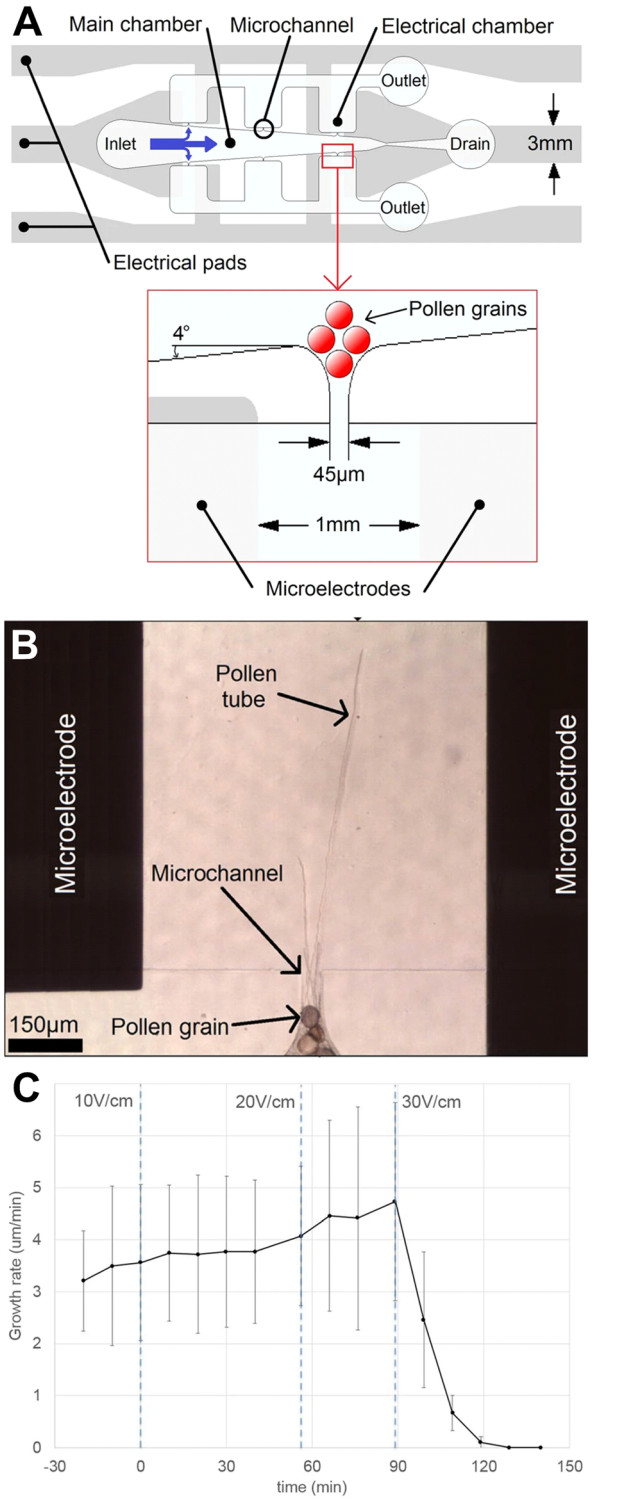

Fig. 6 Single-cell electrical lab-on-chip (ELoC) reveals impact of electrical fields on pollen tube growth. (A) The single-cell ELoC schematic involves trapping pollen grains at the entrance to microchannels 45 μm wide. (B) Upon germination, the pollen tubes grow into a microchamber with microelectrodes on either side and are subjected to DC electric fields. (C) Exposure to weak DC electric fields was found to result in negligible impact on instantaneous growth rate, while exposure to DC electric fields above 30 V cm^{-1} was found to rapidly stop growth. Images produced with modification from ref. 74 under a Creative Commons Attribution License CC-BY 4.0 (http://creativecommons.org/licenses/by/4.0/).

cells.[78] The polysaccharide cell wall facilitates this high internal turgor pressure, and only if the cell wall is pliable enough to deform, is this turgor pressure exerted onto the surrounding substrate. Turgor pressure is thought to be 0.1–0.4 MPa for pollen tubes, as measured using a turgor pressure probe.[79] Pollen tubes have to penetrate very small gaps, so it is important to understand the forces exerted by pollen tubes onto ovules. However, single-cell measurements of force are very difficult to achieve as individual pollen tubes need to be observed as they exert force and are deformed over time. This is difficult with classical plate-based techniques, as the pollen tube needs to be kept in focus.

Microfluidic technology both facilitates focusing on the deformation of a single tip-growing cell at high magnification and manoeuvring cells into suitable positions to encourage turgor pressure to be exerted in a predefined function. Nezhad *et al.* used a modified version of the TipChip to measure the force exerted by growing pollen tubes when squeezing through gaps smaller than their diameter (Fig. 7).[63] Changes in width were measured optically, and, in combination with optical measurements of PDMS deformation, the force exerted by the pollen was calculated using finite element modelling. Using another iteration of the TipChip, Nezhad *et al.* this time used the bending lab-on-chip (BLOC) to measure the Young's modulus (stiffness measurement) of the cell wall surrounding a pollen tube.[78] The device traps a single pollen tube, and media flows perpendicular to the growth of the pollen tube. Optical measurements of the deformation of the pollen tube, combined with computational modelling, allowed the Young's modulus to be calculated. Burri *et al.* took a different approach and combined a microfluidic device with a force sensor, positioned at the output of one of the microchannels.[80] This force sensor quantified the minimum force required for lily and *Arabidopsis* pollen tubes to sense and react to an obstacle. By combining the force readout data with microscopy data, the internal turgor pressure of growing pollen tubes was calculated. This force sensor readout has the potential to ameliorate some of the disadvantages of using deformation calculations to measure force exerted, but both methods give force readouts and turgor pressures with similar literature values to non-microfluidic measurements using probes. Therefore, microfluidic technology has improved upon established methods for chemosensing, electrosensing, and mechanosensing assays using high-resolution real-time imaging of single pollen tube cells.

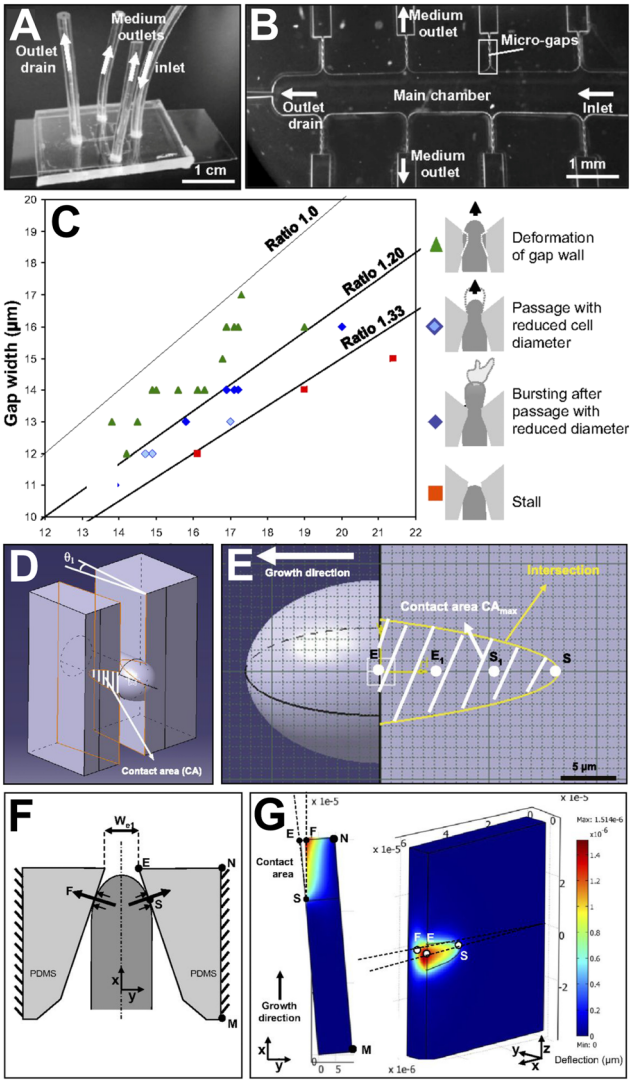

Fig. 7 The TipChip facilitates studies on penetrative forces of pollen tubes using deformation from microgaps and finite element modelling. (A) The TipChip experimental setup illustrating locations of inlets and outlets. (B) The TipChip device design. (C) Variation in *Camellia japonica* pollen tube behaviour was found to depend on the ratio between gap and pollen tube width. Between ratios of 1.00 and 1.20, pollen tubes deform the microgap and pass through (green triangles). Between a ratio of 1.20 and 1.33, pollen tubes pass through with a reduced diameter (light blue diamond) and frequently burst after passing through (dark blue diamond). At a ratio of 1.33 and above, pollen tubes cannot pass through the microgap. (D) Finite element modelling simulating force exertion by the pollen tube on the walls of the microgap. (E) Three-dimensional model of the pollen tube and microgap when the pollen tube is in maximum contact with the microgap. The four points represent reference points for the contact area, starting with S upon initial contact, and finishing at E with exit from the microgap. (F) Top view of the modelled geometry is shown, along with relevant forces acing on the microgap. (G) The deflection of the poly(dimethylsiloxane) (PDMS) material is shown, with respect to the top view (left) and side view (right). The false colour scale represents the degree of sidewall deflection at an effective pressure of 0.15 MPa. Images produced with modification from ref. 63 with permission from Proceedings of the National Academy of Sciences of the United States of America, copyright 2013.

3.2 Microfluidic-assisted studies on moss

Moss species, specifically the model moss *Physcomitrella patens*, have a simple body plan and efficient gene targeting *via* homologous recombination,[81] which has resulted in interest in using *P. patens* as a model organism to study the

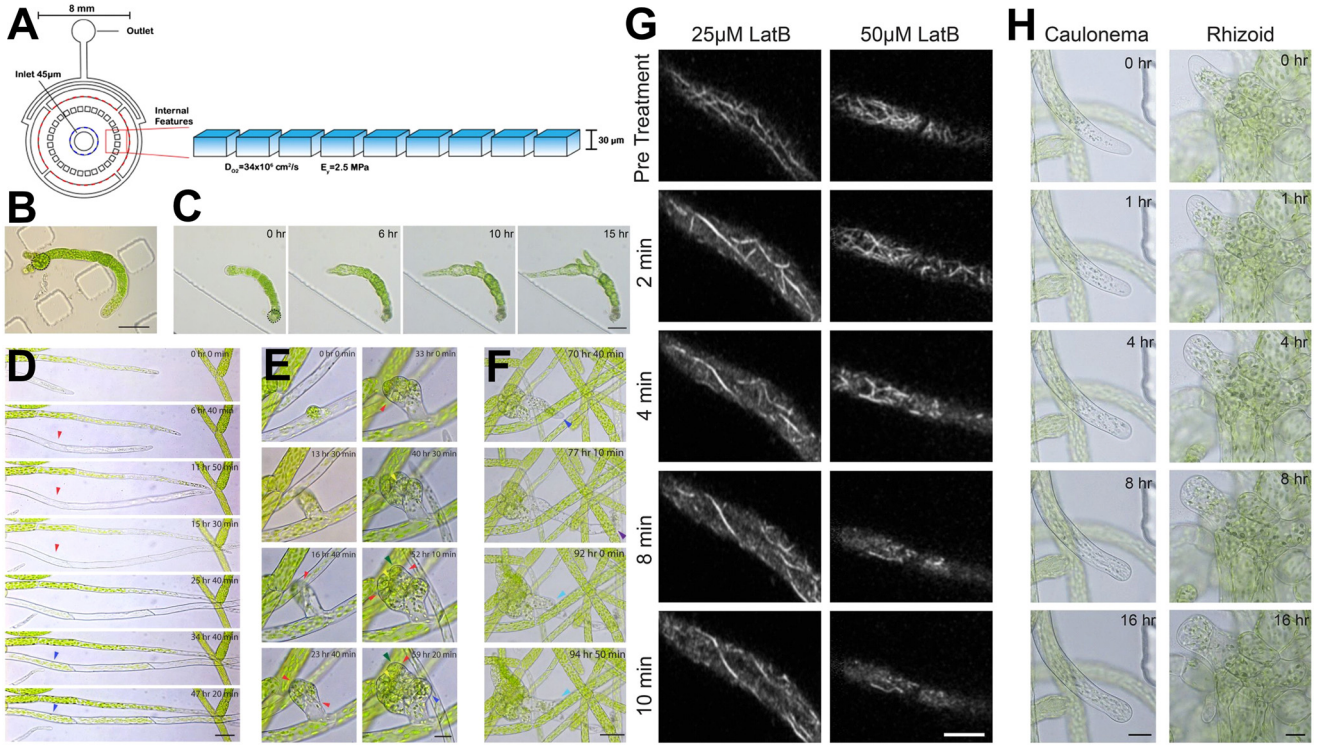

Fig. 8 Microfluidic culture chamber facilitates the observation of developmental events, subcellular dynamics and pharmacological studies. (A) Schematic illustration of the microfluidic culture chamber, with a chamber height of 30 μm to focally confine *Physcomitrella patens*. (B) Protoplast regeneration was observed, as well as subsequent cell division events within 9 days. Scale bar, 50 μm. The initial protoplast is outlined with a black dashed line. (C) Multiple cell division events and branches were observed after protoplast regeneration over 15 hours. Scale bar, 50 μm. Developmental events of *P. patens* were observed inside microfluidic culture chambers. (D) A wild-type caulonemal subapical cell (red arrows) was observed turning into a chloroplast rich cell (blue arrows) after a day. Scale bar, 50 μm. (E) The development of a bud initial from a single cell was observed after 40 hours. Scale bar, 20 μm. A rhizoid initiated from the lateral basal cell (dark blue arrow). (F) Explosion of the rhizoid (purple arrow), with a new rhizoid tip reinitiated after 15 hours. Scale bar, 50 μm. (G) Two different concentrations of an actin-depolymerising drug, latrunculin B (LatB) were used on *P. patens* protonematal subapical cells expressing the actin fluorescent marker LifeAct-mRuby2. Rapid depolymerisation of most actin filaments in both concentrations was observed. (H) Tip growth was inhibited by exposure to the higher concentration of LatB. Images produced with modification from ref. 84 under a Creative Commons Attribution License CC-BY 4.0 (http://creativecommons.org/licenses/by/4.0/).

evolution of developmental processes in land plants at a subcellular level.[82] Moss protonema is the filamentous network formed from a haploid spore, with the apical cell within a filament dividing as the filaments grow radially outward. Within this network, buds form off protonematal filaments and eventually develop into gametophores. Non-microfluidic techniques have been used to study the development of moss protonema, but their utility is limited due to poor focal confinement. In one agar-based technique, protonemata are placed on an agar pad, sealed with a coverslip and imaged immediately. However, cells stop growing after a few hours (presumably due to insufficient gas exchange and limited nutrients). An alternative method involves culturing protonemata in a dish with a coverslip at the bottom covered with a thin film of agar for several days. The protonemata are given enough time to grow close enough to the coverslip and then imaged. The tissue grows well, however, few cells reach the surface of the coverslip, so only a small proportion of the sample can be imaged. Microfluidic technology has assisted in improving culturing and imaging of protonemata. Firstly, sufficient focal confinement means a majority of the sample can be imaged with high-resolution microscopy. Secondly, PDMS is highly air permeable,[83] meaning *P. patens* is able to grow in these devices for several weeks.

Microfluidic device-assisted imaging of moss growth dynamics. Microfluidic technology has been used to investigate the growth dynamics of individual moss protonematal filaments. The first device to do this used a simple circular chamber device design supported by pillars, with a chamber height of 30 μm (Fig. 8A).[84] The authors used brightfield microscopy to observe the growth rates of moss protonemata and showed that a mutant in actin filaments regulation showed slower growth compared to the wild type. Moreover, the authors observed a previously undescribed growth phenomenon, where individual filaments spontaneously underwent rapid growth, twice as fast as other mutant filaments. This was coupled with a change in apical cell morphology, reminiscent of blebbing seen in some mutant pollen tubes. Therefore, microfluidic technology is

useful in facilitating high-resolution brightfield microscopy of moss filament extension, allowing previously unreported growth behaviours to be observed in detail. While Bascom *et al.* used the design of a microfluidic device to contain and grow moss protonemata, the structural features of microfluidic devices can also aid in investigating biological questions.[84] For example, Yanagisawa *et al.* investigated the ability of moss protonema to penetrate constrictions smaller than their diameter, through forcing *P. patens* filaments through constrictions 10 μm wide and 5 μm tall.[68] The diameter of an average protonemal cell is 18–20 μm. The authors observed that protonemal filaments were easily able to cross this constriction, so the authors moved on to smaller 1 μm constrictions. While 43% of protonemal filaments were found to be able to cross this constriction with septa and chloroplasts found on the other side of the gap, when the length of this constriction was extended to 100 μm, none were able to cross. Therefore, moss protonema was found to be able to cross constrictions 5% of the diameter of their filaments, but only if this gap was short. The study by Yanagisawa *et al.*, was used to investigate the behaviour of moss protonema, root hairs, and pollen tubes crossing constrictive gaps.[68] The authors highlight how all three of these tip-growing plant cells can grow through microgaps with their organelles intact, but the length of extension differs between the three groups.

Microfluidic device-assisted studies on moss development. Microfluidic technology allows long-term culturing of moss protonemata and protoplasts, which facilitates the observation of developmental processes over several weeks. Bascom *et al.* used the device discussed above to study moss development (Fig. 8A).[84] The authors achieved focal confinement of *P. patens* protoplasts, and observed developmental events, subcellular studies on moss organelles, moss–chemical interactions, and mutant studies. The authors observed many developmental events: the transformation of a caulonemal (chloroplast deficient) cell into a chloroplast-rich cell, the individual cell division events constituting the development of a bud initial from as single cell, the formation of a tetrahedral meristem cell, and the initiation of a rhizoid from a lateral-basal cell (Fig. 8D–F). A challenge faced by Bascom *et al.* with long-term observations of moss protoplast development regards the control of light conditions.[84] Photoperiodicity (length of night and day cycles) and energy flux (the concentration of light energy impacting the protoplast sample) has been shown to impact physiological development of moss protoplasts,[85] with relative humidity also being important to prevent desiccation. Maintaining the necessary lighting and humidity conditions inside a microscope stage has been a significant limitation in current studies of long-term moss development. Sakai *et al.* sought to overcome this limitation by integrating a custom microscope inside a plant incubator.[57] This allowed the authors to image *P. patens* protoplast development over long time periods at high resolution, and they were able to observe the first division steps and cell wall regeneration, the influence of photoperiodicity on growth, and the induction of leafy buds with cytokinin.

Microfluidic device-assisted imaging of moss cytoskeleton. Microfluidic technology can be combined with complementary techniques such as fluorescent labelling and advanced microscopy techniques to enable studies on moss cytoskeletal regulation. Bascom *et al.* showed the compatibility of their microfluidic device with confocal microscopy and fluorescent labelling by injecting a chemical agent into the central inoculation inlet of the device and observing impacts on actin filaments (2016 Fig. 8).[84] Two different concentrations of an actin-depolymerizing drug, latrunculin B (LatB) were used on *P. patens* protonematal subapical cells expressing the actin fluorescent marker LifeAct-mRuby2 using scanning confocal microscopy, the authors showed rapid depolymerisation of most actin filaments in both concentrations (Fig. 8H), while tip growth was inhibited by exposure to the higher concentration of LatB (Fig. 8G). Moreover, the authors used genetically encoded fluorescent labels targeted to subcellular organelles to show a tip-focused accumulation of Golgi dictyosomes, in agreement with a previous study.[86] Kozgunova and Goshima developed a microfluidic device for highly inclined illumination (HILO) microscopy and optimised the device height to 15 μm to maximise the visible cell surface for HILO imaging.[87] This enabled the authors to observe that the cytoskeleton remodels itself during gametophore regeneration.

3.3 Microfluidics-assisted studies on root hair growth dynamics

The root hair is a terminally differentiated lateral extension of root epidermal cells called trichoblasts. Root hairs display distinct cellular properties from trichoblasts, including cell and vacuole size.[88] Root hair development occurs in three steps: (i) initiation *via* outgrowth from a trichoblast cell, (ii) elongation *via* tip growth, and (iii) maturation when the tip of the root hair cell ceases growing, and is well characterised. In *A. thaliana*, specific genes have been identified as important for root hair development, some of which have been mapped using the RootChip-8S microfluidic device.[89,90] Root hairs are important for both uptaking water and nutrients from the soil, and to anchor the plant to the soil.[91] They also play a crucial role in root–microbe interactions, such as nodulation, where root hairs are involved in the uptake of rhizobia through an infection thread.[92] Generally, root hairs act as the first "point of contact" for any microbe initiating contact with the root surface, as root hair protrusions may cover the root, and extend up to several mm away from the root surface.[88] Nuclear movement within root hairs may be associated with various environmental stimuli such as plant–microbe interactions, nutrient and water uptake, and light response.[93] During root hair growth, nuclear position and movement are tightly regulated by actin and associated proteins in *A. thaliana*.[94] However, due to the small diameter of root hairs (8–20 μm wide depending on the

species), tracking the movement of root hair growth and organelles is difficult with classical plate-based techniques. Microfluidic technology, and fluorescent labelling, allow observation of root hair growth and subcellular dynamics in real time. Using the df-RootChip, Stanley *et al.* showed that root hairs can rapidly modulate their growth rate in response to phosphate availability in a cell-autonomous manner.[28] Yanagisawa *et al.* looked at the ability and subsequent impact on the growth of root hairs to penetrate gaps smaller than the diameter of their cells.[68] The authors found that 77% of *A. thaliana* root hairs were able to penetrate through 1 μm constrictions, suggesting the shape of the root hair apex can be deformed according to its environment. The authors next wanted to see whether root hair nuclei were able to cross the microgaps. The authors used genetically encoded fluorescent *UBQ10pro::H2B-mClover* line, in which the roots and root hair nuclei are fluorescently tagged. This allowed the authors to observe root hair nuclei passing through the 1 μm constrictions. Singh *et al.* investigated root hair nuclear dynamics further by analysing the shape and location of root hair nuclei during and after root hair extension.[58] The authors used *z*-stacks to construct a three-dimensional model of nuclear shape through time. They found that the shape of root hair nuclei is highly dynamic and undergoes significant deformations in its three-dimensional shape. Moreover, the authors found that nuclear aspect ratio (ratio of width to height) increased when root hairs stopped growing (mature phase) compared to the elongation phase. In summary, it has been demonstrated that microfluidic technology can be used in combination with genetically encoded fluorescent labels to correlate organelle and root hair growth dynamics, contributing to a greater understanding of the genetic machinery that underpins root hair development.

4 Microfluidic device-assisted plant protoplast, ovule, and embryo imaging and manipulation

Plant protoplasts are plant cells where the pecto-cellulosic cell wall has been removed, while keeping the cell membrane intact. They can originate from many parts of the plant (typically the mesophyll) and are useful as the removal of the cell wall allows easier genetic manipulation of plant cells using protoplast fusion. In suitable culturing conditions, plant protoplasts can dedifferentiate, divide, and subsequently re-differentiate to eventually reform the whole organism. Therefore, plant protoplasts are useful both as tools for genetic manipulation, and for plant development studies. Investigating plant development using protoplasts requires individual protoplasts to be trapped and observed throughout their developmental process in a high throughput manner, which is difficult in classical approaches using flasks. Microfluidic technology has been shown to offer a method to effectively culture, manipulate, and follow the development process of protoplasts over time. Plant embryos are the early stages of a plant that develops from a fertilised ovule. Studying the development of plant embryos and ovules underpins our understanding of plant development and cell fates. Classical approaches to observe plant ovules and embryos involve dissection, dispersion on a culture dish, and observation using an inverted microscope. Maintaining ovules and embryos in a fixed position over long time periods, as well as manipulating the orientation of ovules and embryos to observe all axes of development is challenging using this approach. Microfluidic technology therefore facilitates the trapping and manipulation of plant ovules and embryos for long-term studies in development.

4.1 Microfluidic device-assisted imaging of plant protoplasts

Microfluidic device-assisted culturing and observation of plant protoplasts. Microfluidic technology has facilitated more efficient culturing of plant protoplasts than classical techniques, such as flasks and agar plates. Ko *et al.* used a simple microfluidic device to culture tobacco protoplasts.[12] The authors were able to show that the microfluidic culture chamber was able to achieve faster protoplast division times, and a lower volume of media required per cell, compared to culturing on agar plates. This is likely a result of constant perfusion of fresh media inside the microfluidic culture chamber.

Moreover, microfluidic technology has facilitated studies on protoplast fusion and cytoskeletal organisation. Typically, investigating which agents may or may not cause fusion of protoplasts is difficult, as timelapse microscopy of individual plant cells is required. Maintaining a suitable environment and keeping cells in focus is challenging in agar-based methods, especially if high-throughput investigation of different chemical agents is desired. Microfluidic technology is a useful way to both culture plant protoplasts and obtain optical data over long time periods. Wu *et al.* showed that microfluidic technology can be used for inducing and observing protoplast fusion events.[95] The authors showed that PEG exposure resulted in chemically induced tobacco protoplast fusion events and were able to achieve a fusion efficiency of 28.8%, which is similar to the fusion efficiency achieved on classical agar plate-based approaches. Seidel *et al.* took this further, by delving deeper into the parameters that impact protoplast fusion efficiency, and by designing a microfluidic device to achieve targeted fusion of individual protoplasts,[96] instead of the batch fusions performed by Wu *et al.*[95] The authors were able to achieve this by trapping individual pairs of *A. thaliana* plant protoplasts in pillar trapping structures. These targeted protoplast fusions allowed Seidel *et al.* to observe the shape of the resulting cell body after fusion to check for abnormal cell shapes, as well as performing vitality staining for up to 10 hours after the suspected fusion event. This enabled the authors to be more confident in assays of fusion efficiency. The authors found that the fusion of protoplasts depended on the PEG concentration of the fusion buffer, the flow velocity inside

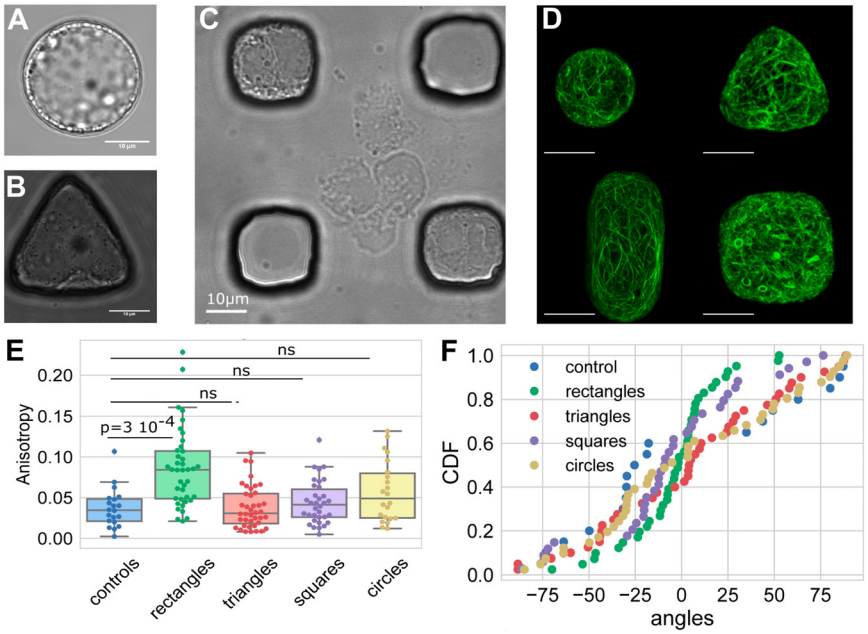

Fig. 9 Custom microfluidic device microwell geometries facilitate studies on protoplast geometry–cytoskeleton interactions. (A–C) Description of the experimental setup. (A) *Arabidopsis thaliana* protoplasts are generated, and (B) trapped in micro-wells of different geometries forming (C) an array. (D) These different protoplast geometries were then used to investigate the impact of geometry on actin network organisation. Image shows protoplasts expressing FABD-GFP reporter confined in microwells of different geometries. Scale bars, 10 μm. (E) Boxplot of the anisotropy of the actin network for each geometry tested. (F) Graph showing the cumulative distribution of the average actin network angle across the different geometries tested. Images produced with modification from ref. 97 under a Creative Commons Attribution License CC-BY 4.0 (http://creativecommons.org/licenses/by/4.0/).

the device, and the osmolarity of the fusion buffer. Moreover, Durand-Smet *et al.* used a microfluidic well device design to test the contribution of cell geometry of *A. thaliana* protoplasts with GFP-fused microtubules to the final organisation of the cytoskeleton.[97] The authors trapped protoplasts in wells of different shapes, which facilitated long-term high-resolution imaging of the cytoskeleton using scanning confocal microscopy. The authors found that the cytoskeleton aligns with the long axis of the cell and developed a model for predicting the importance of microtubule severing to self-organising microtubules (Fig. 9). This study revealed that not only does the cytoskeleton impact the shape of the cell, but that inversely the shape of the cell impacts the cytoskeletal organisation Because the confined cells in the study were unable to elongate and their microtubules were predominantly aligned with the longitudinal axis, this study demonstrates that the transverse microtubule orientation characteristic of elongating plant cells is energy dependent and relaxes to a longitudinal configuration in the absence of elongation. Therefore, microfluidic technology has facilitated the targeted study of protoplast fusion and cytoskeletal structure, allowing individual fusion events and microtubule self-organisation to be observed and assessed in detail. This has contributed to a greater understanding of the parameters required for fusion, facilitating protoplast fusion to be used in a wider range of chemical environments.

Microfluidic device-assisted imaging of plant protoplast–chemical interactions. Not only can microfluidic technology facilitate the extraction of optical data, it can also facilitate the extraction of chemical data with modifications to device design. Xu *et al.* observed the impact of different chemical agents on tobacco protoplast cell wall regeneration using a simple crossed device design. The authors found that the application of an ester inhibited cell wall regeneration compared to a control.[98] Microfluidic devices are typically assembled in an irreversible way and cannot easily be disassembled. This makes obtaining chemical samples difficult. Maisch *et al.* overcame this obstacle through use of a dual-chamber device design.[99] Two chambers are separated by a porous membrane, allowing metabolites but not protoplasts to pass through. In the upper chamber, tobacco protoplasts are cultured. Metabolites then pass through the porous membrane into the lower chamber, and aliquots of media in the lower chamber were collected at specified time intervals for nuclear magnetic resonance (NMR) analysis. This device design allows time-resolved NMR data to be collected from plant protoplasts for the first time. The authors showed the utility of this approach by following the changes in abundance of glucose (as a readout for primary metabolism) and *myo*-inositol (as a readout for signalling) over time. The authors highlight that not only is this a useful way to investigate extracellular metabolites over different growth phases, but that the process could also be scaled up

to be used in the production of pharmacologically useful plant-derived secondary metabolites.

4.2 Microfluidic device-assisted manipulation of plant cells

Microfluidic device-assisted trapping of plant cells. Microfluidic technology facilitates the trapping of plant protoplasts, ovules and embryos for targeted observations of development over time. We have seen how trapping of individual plant protoplasts allows greater confidence in fusion estimates, but trapping is also important for immobilising plant ovules and embryos to ensure fixed positions in long timelapses. Zaban *et al.* used a simple microfluidic device to contain individual *Fucus* protoplasts and observed how different auxin flow regimes impacted the development of the cell axis.[100] Using more complex trapping structures, Park *et al.* designed "microcage" arrays to trap individual *A. thaliana* ovules.[101] The authors tested different widths of these microcages to optimise the number of single ovules trapped for analysis. A trade-off was observed between the percentage of microcages containing at least one trapped ovule, and the occurrence of more than one ovule being trapped per microcage. Microcage widths of 200 μm and 250 μm were chosen for further analysis, as these provided the highest number of single ovules trapped. Even though culture dishes containing the microfluidic devices were frequently transported for observation, the ovules were found to stay stationary and grew inside the microcages without bursting due to the flexibility of PDMS, assisting the observation of ovules over a week. This microcage array was then modified for use with *A. thaliana* embryos and used to facilitate live-cell imaging of developing embryos.[102] Cellular events during embryogenesis were recorded using spinning-disk confocal microscopy. Using *WOX2p::H2B-GFP WOX2p::tdTomato-LTI6b* fluorescently labelled plants, the nucleus and plasma membrane were differentially labelled in the embryo and the suspensor (a temporary organ assisting in the development of the embryo). This allowed tracing of nuclei during cell division events, and therefore cell-division lineage trees of the proembryo, suspensor, and endosperm to be produced. Similarly, Sakai *et al.* designed a microfluidic device to trap individual *P. patens* moss protoplasts and used this device to monitor cell wall regeneration and division of moss protoplasts with fluorescently tagged microtubules (Fig. 10).[57] Therefore, trapping of plant cells (protoplasts, embryos, and ovules) allows individual cellular events to be observed over long time periods without disturbing the orientation and position of the target cell.

Microfluidic device-assisted manipulation of plant cells. Moving beyond trapping of plant cells, microfluidic technology has been utilised to manipulate cells for sorting and analysis. This enables high-throughput analyses on large populations of cells and opens the possibility of studying the interactions between chemical agents on plant cell

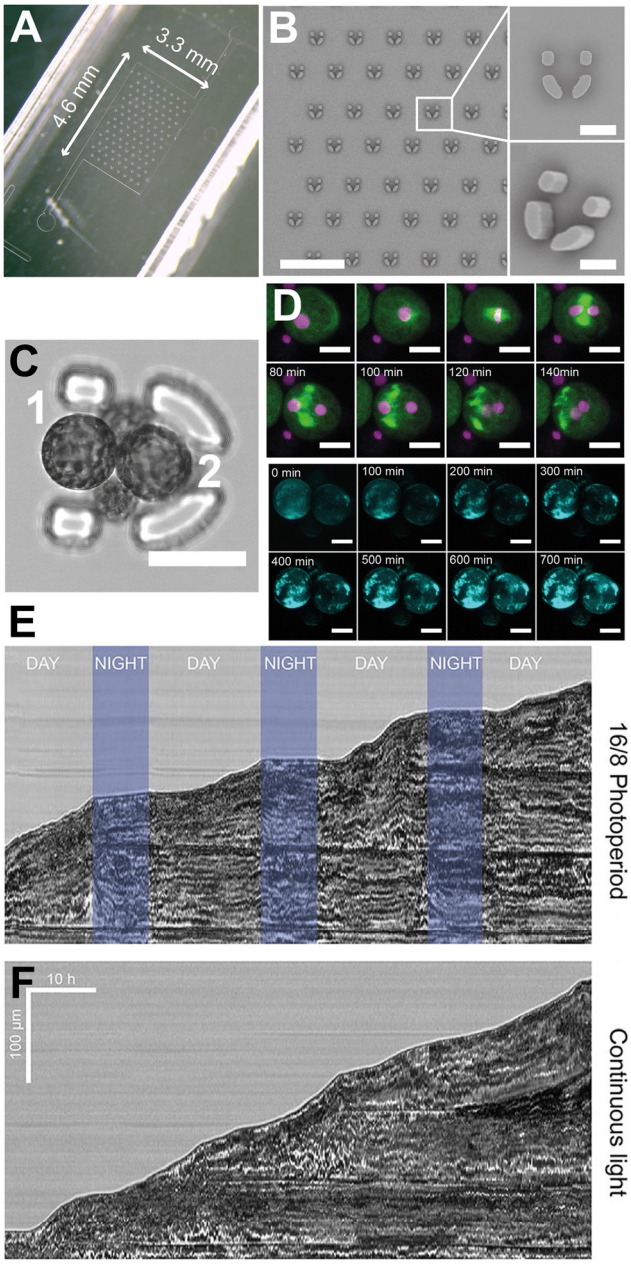

Fig. 10 Microfluidic device for the trapping and observation of plant protoplasts. (A) Photograph of the microfluidic device. (B) SEM micrograph of the device. Scale bar, 500 μm (left), 40 μm (right). (C) Confocal image of a trap containing four H2B-mRFP/microtubules-GFP protoplasts. Scale bar, 40 μm. (D) Protoplasts 1 and 2 are in focus and labelled for subsequent observations. Confocal timelapse (top panel) of the first cell division event of protoplast number 2 (purple: H2B-mRFP, green: microtubules-GFP). The GFP channel is in maximum projection mode. Scale bar, 20 μm. Maximum projection confocal timelapse (bottom panel) of the cell wall regeneration around protoplasts 1 and 2 using the dye calcofluor white. Scale bar, 20 μm. Kymograph of the protonema growth under a 16–8 photoperiod (E) and under continuous light (F) using a custom microscope contained within a plant incubator. Images produced with modification ref. 57 under a Creative Commons Attribution License CC-BY 4.0 (http://creativecommons.org/licenses/by/4.0/).

populations. Kumar *et al.* leveraged digital microfluidic technology to manipulate droplets containing plant protoplasts.[103] Digital microfluidics is a platform for manipulating droplets using a set of insulated electrodes, and allows droplets to be moved, stored, mixed, reacted and analysed. While not typically applicable to the study of plant cells, protoplasts can be stored inside droplets, which allows digital microfluidic techniques to be leveraged. The authors utilised this ability to fuse droplets containing different chemical agents to investigate the water permeability coefficients of *A. thaliana* protoplasts. The ability to physically move protoplasts can also be achieved through electrode-assisted droplet deformation (Fig. 11).[104] Individual *Marchantia* protoplasts were encapsulated and observed inside microfluidic channels. Selective sorting between YFP-expressing and wild type protoplasts was achieved automatically by deforming droplets expressing YFP using two electrodes exerting a dielectric force, pushing the droplet into the "positive" channel. Therefore, manipulating individual protoplasts facilitates targeted application of chemical agents, and precise sorting.

5 Microfluidic device-assisted plant screening

Optimising environmental conditions for plant growth and development is important for both plant and agricultural sciences. Due to the large number of environmental parameters plants are exposed to that influence growth and development such as temperature, nutrients, hormones, moisture and other chemical agents, high throughput phenotyping is necessary. Classical agar and soil mesocosm approaches for assessing the impact of a chemical agent on a plant phenotype involves preparing plates or pots of varying concentrations of the chemical agent, spotting seeds and observing plants over time, while incubating in a plant incubation chamber or growth room. This is space and time intensive, and not feasible for studies involving many different chemical agents. While more efficient methods of quantifying root traits using automated root analysis software[105] has improved the efficiency of phenotyping some plant traits, a major limitation is the lack of multiplexing (the ability to test multiple chemical agents simultaneously) in a small environmentally controlled space. Efficient seed/seedling trapping and perfusion control makes microfluidic technology suitable to fill this methodological gap and facilitate high-throughput phenotyping of plant seedlings and organs.

5.1 Microfluidic device-assisted high-throughput plant phenomics

Microfluidic technology facilitates high throughput imaging of seedling morphology at the organ and tissue level over a range of chemical conditions. High-throughput observation of changes in seedling morphology is used to link genotypes to phenotypes, potentially uncovering the mechanisms behind plant disease. Jiang *et al.* modified the design philosophy of early RootChip devices (Section 2) to allow for a vertically orientated device for gravitropism, and to allow seed germination to be monitored on chip (Fig. 12).[26] The authors used hydrodynamic trapping to ensure a single *Arabidopsis* seed was trapped per well, and were able to

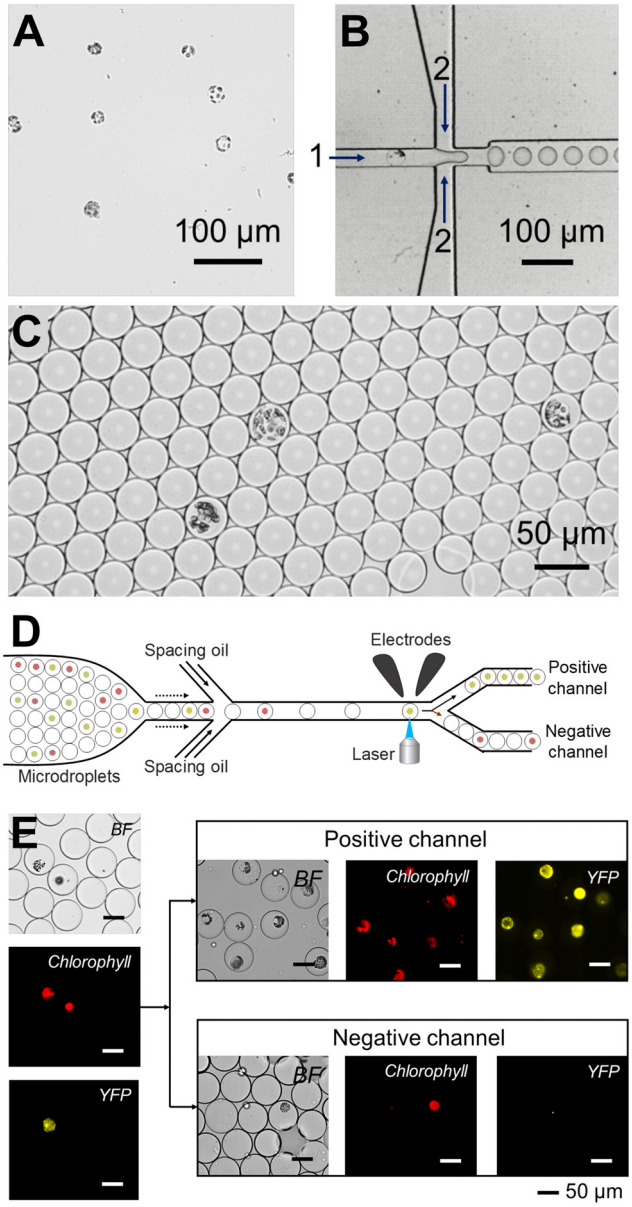

Fig. 11 Droplet microfluidic technology facilitates precise manipulation of individual plant protoplasts. (A) Droplet microfluidic technology was used to encapsulate *Marchantia polymorpha* protoplasts using (B) a flow-focusing microfluidic device. (C) Image showing *M. polymorpha* protoplasts encapsulated into microdroplets. (D) Schematic of microfluidic device used to sort *M. polymorpha* protoplasts. (E) Representative brightfield and fluorescent micrographs used for sorting *M. polymorpha* protoplasts into positive and negative channels using their mVenus fluorescence intensity. Images produced with modification from ref. 104 under a Creative Commons Attribution License CC-BY 4.0 (http://creativecommons.org/licenses/by/4.0/).

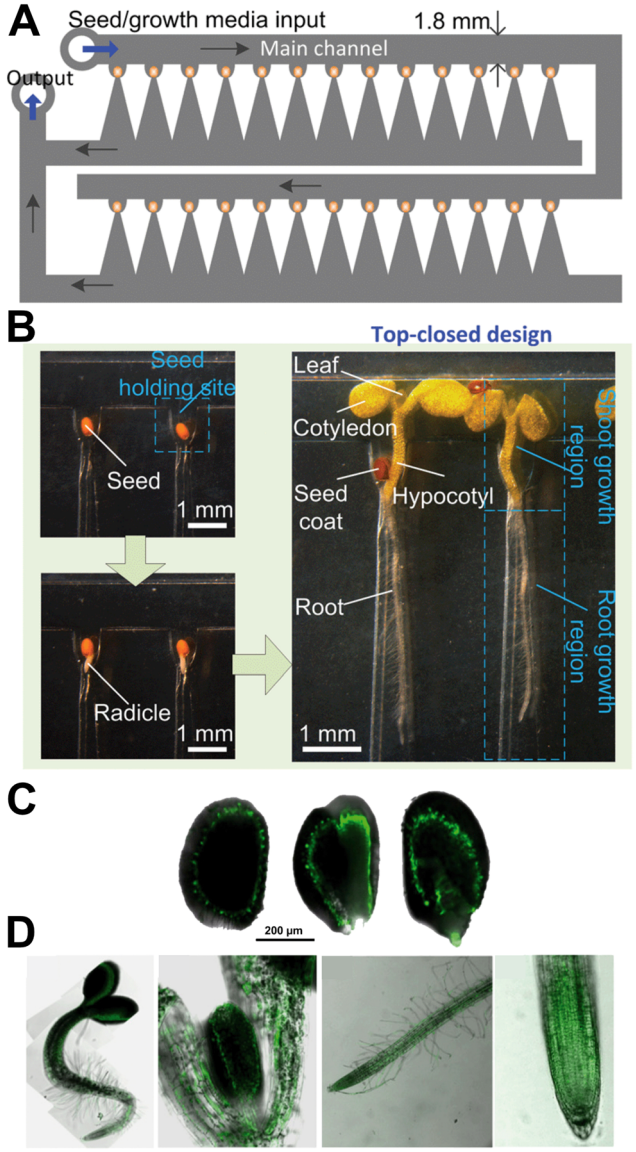

Fig. 12 Microfluidic technology facilitates high-throughput phenotyping of plant germination and development. (A) Schematic illustration of the plant chip. (B) The device hydrodynamically traps *Arabidopsis thaliana* seeds in "holding sites". Micrographs show in-chip seed germination and development, with major plant organs labelled. (C) *IM GFP A. thaliana* plants were grown inside the plant chip to follow *IM* expression, and confocal scanning laser microscopy was used to show seed germination over 18 hours post germination. (D) *IM* expression in several plant organs was also monitored. Left to right: 1 day old seedlings at a magnification of 10×, 5 day old leaves at 20×, 5 day old root at 10×, 5 day old root tip at 40×. Images produced with modification from ref. 26 with permission from the Royal Society of Chemistry, copyright 2014.

phenotype different *A. thaliana* mutants, including cellular morphology using genetically fluorescent labels inside the device. The authors also show a variant of the device with an open top, that is shown to facilitate longer term growth studies of *A. thaliana* seedlings of up to 15 days, enabling later developmental stages to be investigated. This device is space efficient, but the device can only investigate one concentration of chemical agent (here tested using different media) at a time. To enable more precise control over the concentration of chemical agents, Jiang *et al.* modified the device to integrate a hormone concentration gradient generator (CGG).[106] This was shown to offer fine control of concentration gradients through splitting, combining and mixing of two input concentrations, delivering 8 different output concentrations to the 8 seedlings in the plant chip. This technology is best suited for investigating the first developmental processes in small plants such as the model *A. thaliana*, where soil mesocosms are not required. Microfluidic technology is useful not only in high-throughput observation of plant phenotypes, but also in efficiently generating stimulus gradients. For example, Wang *et al.* used an inclined microfluidic device on top of a thermos-electric cooling plate, to generate a temperature gradient across an *A. thaliana* plant.[107]

5.2 Microfluidic device-assisted high-throughput imaging of gene expression

High-throughput plant phenotyping microfluidic devices can be combined with complementary techniques such as genetically encoded reporters and nucleic acid sequencing to leverage deeper insights into plant biology. Busch *et al.* introduced the RootArray, which can accommodate 64 *A. thaliana* seedlings, and has separate root and shoot compartments, which are supplied with liquid and gas respectively (Fig. 13).[35] The authors used confocal microscopy to image 12 different transgenic reporter lines over several days and later reconstructed three-dimensional reconstructions from stitched high-resolution images. This allowed the authors to capture detailed expression maps of the 12 reporter constructs under different environmental conditions, allowing changes in gene expression to be linked to environmental conditions in a high-throughput manner.

6 Outlooks and future research

6.1 Integration and iteration of microfluidic devices drives progress in plant microfluidics

The field of microfluidics has advanced plant sciences greatly in the past two decades, from single straight channel RootChip designs[22] and single chamber devices for protoplast culturing,[12] to microfluidic devices integrating on-chip chemical analysis,[30] and force measurements.[63] This trend of increased integration of previously off-chip experimental components into microfluidic devices has the benefit of increased miniaturisation of experimental components, finer spatial control of the internal microenvironment, and the facilitation of novel on-chip assays. Taking this further, microfluidic studies for plant sciences would benefit from the integration of a broader range of sensors for environmental measurements such as pH, temperature, and oxygen concentrations, as has been implemented in adjacent microfluidic fields[108] and recently in root–rhizosphere interactions.[109] However, increasing

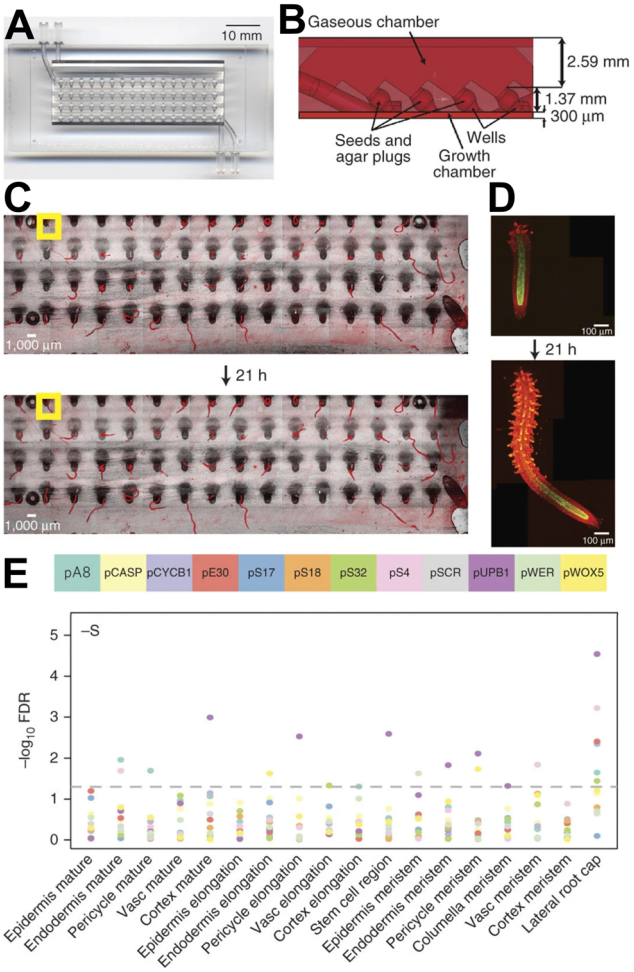

Fig. 13 The RootArray microfluidic device facilitates high-throughput imaging of gene expression in *Arabidopsis thaliana* plants. (A) The RootArray, consisting of 64 individual wells. (B) Cross-section of the RootArray shows that each well connects the upper and lower chambers, enabling the roots to extend into the liquid chamber while the shoots grow upward into the gaseous chamber. The top and bottom boundaries of the illustration represent coverslips, which seal the RootArray device. Root growth can be imaged over multiple hours. (C) A representative low-resolution overview image. (D) A stitched high-resolution image of a single root captured at two different time points. (E) A gene expression map under sulphur-deficient medium obtained through microscopy acquisition of GFP reporter constructs and semi-automated image acquisition and analysis steps. Different tissue types are displayed along the *x*-axis, while the *y*-axis shows the $-\log_{10}$ false discovery rates (FDRs) representing changes in gene expression relative to expression in the standard medium for each color-coded reporter gene. The dashed horizontal line marks the 5% FDR significance threshold. "Vasc" denotes vasculature. Images produced with modification from ref. 35 under a Creative Commons Attribution License CC-BY 4.0 (http://creativecommons.org/licenses/by/4.0/).

integration also increases the complexity of manufacturing and using microfluidic devices. Hence, the benefits of further integration of components into microfluidic devices must be weighed against the increased time investment, cost, and barrier to entry. Another factor contributing to progress in plant microfluidics concerns the reuse and iteration of existing microfluidic device designs, which has allowed useful device designs, such as the RootChip[22] and the dual-flow-RootChip,[28] to be reused or modified by other research groups.[27,36,38–41,51,90,110]

6.2 Root–electric interaction studies

Interest in the field of root–electric interactions peaked between the 1960s and 1990s, with the discovery of a root electric signature.[77,111] More recently, plant bioelectricity gained more attention with a variety of discoveries, including the importance of electric fields in pollination,[112] electric field influence on pollen tube targeting, root electrotropic responses[113] and the use of external electric fields to reduce root pathogen infection.[114] Microfluidic technology has the potential to advance this area. Control and manipulation of microenvironments allow for more controlled electric field application and prevent media evaporation, while the use of very small amount of liquids significantly reduces Joule heating and can help stabilise ion currents.[115] Microfluidic technology, together with the standardisation of the instruments and media used to measure electric fields and currents,[77] could provide significant novel insights into plant bioelectricity.

6.3 Rhizosphere-on-a-chip technology

Beyond bipartite root–microbe interactions, there is a need to develop generalised simplified rhizospheric ecosystems to study soil community dynamics.[116] While a microfluidic device has successfully shown soil microbe community dynamics for soil and associated microbes,[117] the inclusion of plant roots has not yet been achieved for reasons discussed above. Incorporating plant roots into simplified rhizospheric systems is an important goal to ensure a more representative soil ecosystem inside microfluidic devices, and to investigate the impact of root exudates on soil microbes. Soil structure is a key part of replicating simplified soil ecosystems on-chip. The field of transparent soil particles is a relatively new field that is advancing rapidly, where artificial soils are engineered with varying physiochemical properties to study specific aspects of soil structure.[118] Super-absorbent polymers (SAPs) have been used to replicate the structural complexity of soil, while maintaining optically transparency for microscopy.[119] While SAP-based systems have not yet been incorporated into microfluidic devices, the relationship between soil structure and the rhizosphere has been investigated using etched structures to replicate soil particles in plant devices,[30,31] as well as photolithography for investigating bacterial accumulation in complex porous media.[120] The next steps are to incorporate displaceable soil particles into microfluidic devices, which is more representative of edaphic environments. Therefore, further research is needed to build a picture of how the relationship between soil properties, root exudates, and soil microbes functions in simplified ecosystems. This research could uncover how unique biological niches are generated in soil

through the relationship between roots, root exudates, and soil properties, helping to clarify global distributions of soil biodiversity.

6.4 Root–hyphal interaction studies

Microfluidic technology is well-suited to follow the first few weeks of root–microbe interactions due to focal confinement the root, and potentially the microbial partner(s). Microfluidic technology for root–bacteria interactions[23,45] and root–oomycete interactions[39,44,47] has allowed researchers to delve deeper into the spatial relationships between roots and these two microbial taxa than classical approaches have allowed. Looking forward, there is a need to design microfluidic devices to study root–hyphal interactions by incorporating filamentous fungi and oomycetes into microfluidic devices.[15,116] This would facilitate a new approach to study root–pathogen and root–mutualist interactions in real-time at cellular resolution and could have impacts on plant health and nutrition. While microfluidic devices have been successfully used to study the behaviour of fungal and oomycete spores and hyphae independently of plant roots,[121,122] filamentous root interactors have not yet been incorporated into these simplified ecosystems due to plant roots requiring taller channel heights, which prevents focal confinement of smaller soil microbes. Very recently, new microfluidic technologies have been developed that allow the growth of individual hyphae of arbuscular mycorrhizal fungi (AMF) within confined microchannels for the first time.[123,124] Progress has also been made in non-invasive monitoring of root–hyphal interactions in roots using transparent media,[125] but non-invasive monitoring of the initiation of symbiosis between filamentous microbes and roots is not yet possible due to difficulties in imaging hyphal approach towards a root in real time. To bridge this technological challenge, progress in microfabrication techniques are needed to combine small (<10 μm) microchannels for focal confinement of hyphae with much larger (>200 μm) channels. While this combination of "thick and thin" microchannels has been achieved for focally confining root hairs of *A. thaliana*,[58,68] microchannels for accommodating roots of relevant model plants such as *Medicago truncatula* and *Nicotiana benthamiana* require root microchannels significantly thicker than 200 μm. Future progress in microfabrication techniques to accommodate these larger model plants would also allow larger crop plants such as wheat and rice to more easily be incorporated into microfluidic devices. Studying crop plants directly instead of more established model plants, allows species-specific mechanisms to be investigated, and has direct applications to agriculture.

6.5 Millifluidic devices

As explored in Box 1, there are various alternatives to standard photolithography for manufacturing microfluidic devices with layer heights taller than 200 μm, each with specific advantages and drawbacks. 3D printing is limited in manufacturing small feature sizes (less than 15 μm), but the cost of high-quality fused deposition modelling (FDM) and stereolithography (SLA) 3D printing machines has decreased rapidly in the last decade, reducing the barrier to entry for the adoption of microfluidic technology. This has resulted in the production of millifluidic devices (devices where the smallest dimension of the device is most easily measured in millimetres), which have facilitated studies into root–rhizosphere interactions. For example, the EcoFAB device,[126] has allowed researchers to monitor root–rhizosphere interactions in a repeatable way by publishing guides on fabricating the EcoFAB device.[126] This has resulted in modified EcoFAB devices such as the RootTRAPR device[127] and Imaging EcoFAB. Therefore, while an exhaustive discussion of plant millifluidic technology is outside the scope of this review, many design principles and manufacturing techniques are applicable to microfluidic technology.

6.6 Droplet and digital microfluidic technologies

Beyond microfluidic technology to study roots and soil, we have seen how microfluidic technology has contributed greatly to understanding how plant cells, particularly pollen tubes, function. The next frontier in this field involves translating advances from the fields of droplet and digital microfluidics to provide greater control and analytical ability to study plant cells. The former involves encapsulating (single) cells inside water-in-oil microdroplets, with the latter using electric fields to manipulate discrete microdroplets; both approaches allow precise control of droplets (*i.e.*, fusion, splitting, dispensing *etc.*) in an automated way. Digital microfluidic platforms have already been used extensively for mammalian cell cultures,[128] with only one example of this technique being applied to measure water permeability of isolated plant protoplasts.[103] Droplet microfluidic technology has been applied in producing microfluidic bioreactors for the production of economically important plant-derived compounds.[129] Automated manipulation and analysis of individual plant protoplasts could assist with high-throughput plant genotyping and phenotyping, paving the way to characterise the phenome of genetic models such as *A. thaliana*. Moreover, root and droplet microfluidic technology could be integrated, for example to encapsulate plant root exudates to provide a spatially explicit, time-resolved snapshot of the root secretome.

6.7 Extracting samples from microfluidic devices

A common challenge in utilising microfluidic technology for the study of plants is the difficulty in extracting samples from inside microfluidic devices for further chemical analysis. Throughout, we have seen different approaches used to overcome this challenge. Chai *et al.* constructed an openable and resealable device, allowing samples to be extracted at coarse spatial resolution.[42]

Aufrecht *et al.* replaced a chemically impermeable glass coverslip with a selectively permeable PETE membrane, allowing on-device analysis of amino acid profiles.[30] Maisch *et al.* separated a fluid extraction channel from the culture channel with a semi-permeable membrane, allowing cell exudates to diffuse through and be collected at specified time points.[99] Finally, Dai *et al.* measured dissolved oxygen and pH inside a microfluidic device using microeletrode sensors, and at regularly spaced intervals collected soil pore water.[109] All approaches have varying trade-offs with respect to the kind of data that can be extracted and impact on optical data. These tradeoffs should be carefully considered, and microfluidic devices should be designed from inception to interface with appropriate extraction techniques when required.

6.8 Advancing image analysis

Another common challenge is extracting biological inferences from the imaging data collected during microfluidic experiments. Simple observations of behaviours are useful, but quantification of complex behaviours is difficult to achieve manually using classical analytical techniques such as the open source software package ImageJ.[130] More advanced algorithms to remove background noise, track biological objects, and quantify network traits have had limited success with image data generated from microfluidic devices, as these specialised algorithms are trained on microscopy data not obtained from microfluidic devices, which can have different image parameters. More generalised artificial intelligence tools such as the Segment Anything Model[131] may prove useful in increasing the throughput of image analysis pipelines and make quantitative measures of biological traits possible.

6.9 Leaf-on-a-chip

Lastly, a notable absence in the field of microfluidic technology for plant sciences is the study of leaves. While leaves are more easily observed and analysed using classical approaches than their belowground root counterparts, microfluidic technology can and has started to provide useful benefits in studying these organs. For example, a microfluidic device was used to monitor electro-mechanical data across stomata *in planta*.[132] PDMS imprints of leaves have also been used to investigate the effect of leaf topography on the microbiology of the leaf phyllosphere.[133] Using microfluidic technology to further understand leaf functioning at the microscale could contributing to a greater understanding of the dynamics of photosynthesis, possibly resulting in efficiency gains in the leaves of genetically transformed crops. Generating a "leaf-on-a-chip" simplified leaf model could assist in selectively breeding for traits to improve leaf function, and aid areas outside of plant sciences by applying what makes leaves so efficient in their water and resource use to engineered products such as valves.[134]

6.10 Accessibility in plant microfluidics

The field of plant microfluidics is now twenty years old. While significant progress has been made during this time, the field is still relatively new. Except for a handful of device designs discussed previously, most microfluidic device designs have been published once only, for a specific use case, without further adoption by the scientific community. As the field matures in the following twenty years of plant microfluidic research, a significant challenge remains of making plant microfluidics widely accessible to the broader plant sciences community through device standardisation. While at first glance, standardisation and customisation may seem at odds, further standardisation and customisation can be achieved in tandem. This could be achieved through further standardisation of existing successful device designs, targeted efforts to increase usability, and a larger focus on making device designs and manufacturing protocols open and accessible. Meanwhile, freedom of customisation can be pursued for novel experimental designs and capabilities. In this way, the next twenty years of plant microfluidic will drive many more advances in plant sciences.

Author contributions

Conceptualisation: L. C., C. E. S.; funding acquisition: C. E. S.; supervision: C. E. S.; visualisation: L. C., C. E. S.; writing – original draft: L. C., E. M.; writing – review & editing: L. C., E. M., C. E. S.

Conflicts of interest

None declared.

Data availability

No primary research results, software or code have been included and no new data were generated or analysed as part of this review.

Acknowledgements

We acknowledge financial support from the Leverhulme Centre for the Holobiont (RC-2021-058; funding awarded to C. E. S. to support L. C.'s PhD studentship), as well as from the Department of Bioengineering at Imperial College, London.

References

1 M. R. Appidi, A. N. Bible, D. L. Carper, S. S. Jawdy, R. J. Giannone, R. L. Hettich, J. Morrell-Falvey and P. E. Abraham, *Mol. Plant-Microbe Interact.*, 2022, **35**, 639–649.
2 M. Oliva and C. Dunand, *New Phytol.*, 2007, **176**, 37–43.
3 W. Xu, G. Ding, K. Yokawa, F. Baluška, Q.-F. Li, Y. Liu, W. Shi, J. Liang and J. Zhang, *Sci. Rep.*, 2013, **3**, 1273.
4 D. J. Harrison, A. Manz, Z. Fan, H. Luedi and H. M. Widmer, *Anal. Chem.*, 1992, **64**, 1926–1932.

5 U. A. Gurkan, D. K. Wood, D. Carranza, L. H. Herbertson, S. L. Diamond, E. Du, S. Guha, J. Di Paola, P. C. Hines, I. Papautsky, S. S. Shevkoplyas, N. J. Sniadecki, V. K. Pamula, P. Sundd, A. Rizwan, P. Qasba and W. A. Lam, *Lab Chip*, 2024, **24**, 1867–1874.
6 C. Chircov and A. M. Grumezescu, *Micromachines*, 2022, **13**, 164.
7 A. Groisman, C. Lobo, H. Cho, J. K. Campbell, Y. S. Dufour, A. M. Stevens and A. Levchenko, *Nat. Methods*, 2005, **2**, 685–689.
8 P. J. Lee, N. C. Helman, W. A. Lim and P. J. Hung, *BioTechniques*, 2008, **44**, 91–95.
9 R. Davidsson, B. Johansson, V. Passoth, M. Bengtsson, T. Laurell and J. Emnéus, *Lab Chip*, 2004, **4**, 488–494.
10 J. Enger, M. Goksör, K. Ramser, P. Hagberg and D. Hanstorp, *Lab Chip*, 2004, **4**, 196–200.
11 C. Sakamoto, N. Yamaguchi and M. Nasu, *Appl. Environ. Microbiol.*, 2005, **71**, 1117–1121.
12 J.-M. Ko, J. Ju, S. Lee and H.-C. Cha, *Protoplasma*, 2006, **227**, 237–240.
13 M. Meier, E. M. Lucchetta and R. F. Ismagilov, *Lab Chip*, 2010, **10**, 2147–2153.
14 M. Elitaş, M. Yüce and H. Budak, *Analyst*, 2017, **142**, 835–848.
15 C.-F. Kaiser, A. Perilli, G. Grossmann and Y. Meroz, *J. Exp. Bot.*, 2023, **74**, 3851–3863.
16 A. S. Nezhad, *Lab Chip*, 2014, **14**, 3262–3274.
17 N. Yanagisawa, E. Kozgunova, G. Grossmann, A. Geitmann and T. Higashiyama, *Plant Cell Physiol.*, 2021, **62**, 1239–1250.
18 L. Philippot, J. M. Raaijmakers, P. Lemanceau and W. H. van der Putten, *Nat. Rev. Microbiol.*, 2013, **11**, 789–799.
19 W. Xu, G. Ding, K. Yokawa, F. Baluška, Q.-F. Li, Y. Liu, W. Shi, J. Liang and J. Zhang, *Sci. Rep.*, 2013, **3**, 1273.
20 B. D. Gruber, R. F. H. Giehl, S. Friedel and N. von Wiren, *Plant Physiol.*, 2013, **163**, 161–179.
21 S. Okumoto, *Curr. Opin. Biotechnol.*, 2010, **21**, 45–54.
22 G. Grossmann, W.-J. Guo, D. W. Ehrhardt, W. B. Frommer, R. V. Sit, S. R. Quake and M. Meier, *Plant Cell*, 2011, **23**, 4234–4240.
23 M.-F. Noirot-Gros, S. V. Shinde, C. Akins, J. L. Johnson, S. Zerbs, R. Wilton, K. M. Kemner, P. Noirot and G. Babnigg, *Front. Plant Sci.*, 2020, **11**, 408.
24 H. H. Chai, F. Chen, S. J. Zhang, Y. D. Li, Z. S. Lu, Y. J. Kang and L. Yu, *Lab Chip*, 2019, **19**, 2383–2393.
25 G. Dupouy, G. Singh, L. M. Schmidt-Speicher, E. Hoffmann, S. Baudrey, R. Ahrens, A. E. Guber, M. Ryckelynck, E. Herzog, M.-E. Chabouté and A. Berr, in *Methods for Plant Nucleus and Chromatin Studies: Methods and Protocols*, ed. C. Baroux and C. Tatout, Springer US, New York, NY, 2025, pp. 223–245.
26 H. Jiang, Z. Xu, M. Aluru and L. Dong, *Lab Chip*, 2014, **14**, 1281–1293.
27 V. Lanquar, G. Großmann, J. L. Vinkenborg, M. Merkx, S. Thomine and W. B. Frommer, *New Phytol.*, 2014, **202**, 198–208.
28 C. E. Stanley, J. Shrivastava, R. Brugman, E. Heinzelmann, D. van Swaay and G. Grossmann, *New Phytol.*, 2018, **217**, 1357–1369.
29 P. Bastian, A. Chavarría-Krauser, C. Engwer, W. Jäger, S. Marnach and M. Ptashnyk, *J. Theor. Biol.*, 2008, **254**, 99–109.
30 J. Aufrecht, M. Khalid, C. L. Walton, K. Tate, J. F. Cahill and S. T. Retterer, *Lab Chip*, 2022, **22**, 954–963.
31 I. A. Atoloye, D. Herrera, D. Veličković, C. S. Clendinen, K. Tate, A. Bhattacharjee, J. Aufrecht, T. Zeng, D. Rai and A. Bhowmik, *Rhizosphere*, 2025, **34**, 101099.
32 M. Moussus and M. Meier, *Lab Chip*, 2021, **21**, 2557–2564.
33 C.-H. Lin, G.-B. Lee, B.-W. Chang and G.-L. Chang, *J. Micromech. Microeng.*, 2002, **12**, 590.
34 R. Su, F. Wang and M. C. McAlpine, *Lab Chip*, 2023, **23**, 1279–1299.
35 W. Busch, B. T. Moore, B. Martsberger, D. L. Mace, R. W. Twigg, J. Jung, I. Pruteanu-Malinici, S. J. Kennedy, G. K. Fricke, R. L. Clark, U. Ohler and P. N. Benfey, *Nat. Methods*, 2012, **9**, 1101–1106.
36 A. M. Jones, J. Å. Danielson, S. N. ManojKumar, V. Lanquar, G. Grossmann and W. B. Frommer, *eLife*, 2014, **3**, e01741.
37 M. Fendrych, M. Akhmanova, J. Merrin, M. Glanc, S. Hagihara, K. Takahashi, N. Uchida, K. U. Torii and J. Friml, *Nat. Plants*, 2018, **4**, 453–459.
38 C. Allan, A. Tayagui, R. Hornung, V. Nock and C.-N. Meisrimler, *Front. Plant Sci.*, 2023, **13**, 1040117.
39 C. Allan, Y. Sun, S. C. Whisson, M. Porter, P. C. Boevink, V. Nock and C.-N. Meisrimler, *Lab Chip*, 2024, **24**, 5360–5373.
40 N. F. Keinath, R. Waadt, R. Brugman, J. I. Schroeder, G. Grossmann, K. Schumacher and M. Krebs, *Mol. Plant*, 2015, **8**, 1188–1200.
41 C. Brost, T. Studtrucker, R. Reimann, P. Denninger, J. Czekalla, M. Krebs, B. Fabry, K. Schumacher, G. Grossmann and P. Dietrich, *Plant J.*, 2019, **99**, 910–923.
42 H. Chai, C. Feng, K. Ning, W. Sun and L. Yu, *Sens. Actuators, B*, 2023, **392**, 134107.
43 M. G. A. van der Heijden, R. D. Bardgett and N. M. van Straalen, *Ecol. Lett.*, 2008, **11**, 296–310.
44 A. Parashar and S. Pandey, *Appl. Phys. Lett.*, 2011, **98**, 263703.
45 H. Massalha, E. Korenblum, E. Korenblum, S. Malitsky, O. H. Shapiro and A. Aharoni, *Proc. Natl. Acad. Sci. U. S. A.*, 2017, **114**, 4549–4554.
46 J. M. Conway, P. J. Martinez, E. D. Wilson, N. M. Del Risco and J. L. Dangl, in *Tissue Morphogenesis: Methods and Protocols*, ed. C. M. Nelson, Springer US, New York, NY, 2024, pp. 213–228.
47 C. Cohen, F. X. Gauci, X. Noblin, E. Galiana, A. Attard and P. Thomen, *Phys. Rev. E*, 2025, **111**, 024411.
48 M. Watt, W. K. Silk and J. B. Passioura, *Ann. Bot.*, 2006, **97**, 839–855.
49 B. Borer, R. Tecon and D. Or, *Nat. Commun.*, 2018, **9**, 769.
50 H. Zhang, X. Yan, M. Zhang, Y. Zhao, S. Jiang, Y. Jiang, Y. Wei, Y. Zhang and L. Sun, *J. Agric. Food Chem.*, 2025, **73**(48), 30895–30903.

51 S. Liu, S. Strauss, M. Adibi, G. Mosca, S. Yoshida, R. D. Ioio, A. Runions, T. G. Andersen, G. Grossmann, P. Huijser, R. S. Smith and M. Tsiantis, *Curr. Biol.*, 2022, **32**, 1974–1985.e3.
52 K. Agarwal, S. K. Mehta and P. K. Mondal, *Lab Chip*, 2024, **24**, 3775–3789.
53 J. Li, M. Notaguchi, I. Kanno and H. Hida, *IEEJ Trans. Electr. Electron. Eng.*, 2025, **20**, 1134–1140.
54 P. Vinet, V. Audemar, P. Durand-Smet, J.-M. Frachisse and S. Thomine, *bioRxiv*, 2025, preprint, DOI: 10.1101/2025.10.22.683952.
55 C. M. Rounds and M. Bezanilla, *Annu. Rev. Plant Biol.*, 2013, **64**, 243–265.
56 M. Ghanbari, A. S. Nezhad, C. G. Agudelo, M. Packirisamy and A. Geitmann, *J. Biosci. Bioeng.*, 2014, **117**, 504–511.
57 K. Sakai, F. Charlot, T. L. Saux, S. Bonhomme, F. Nogué, J. Palauqui and J. Fattaccioli, *Plant Methods*, 2019, **15**, 79.
58 G. Singh, D. Pereira, S. Baudrey, E. Hoffmann, M. Ryckelynck, A. Asnacios and M.-E. Chabouté, *Plant J.*, 2021, **108**, 303–313.
59 J. H. Williams, *Proc. Natl. Acad. Sci. U. S. A.*, 2008, **105**, 11259–11263.
60 F. Bou Daher, Y. Chebli and A. Geitmann, *Plant Cell Rep.*, 2009, **28**, 347–357.
61 R. Palanivelu and T. Tsukamoto, *WIREs Dev. Biol.*, 2012, **1**, 96–113.
62 W. J. Uwate, J. Lin, K. Ryugo and V. Stallman, *Can. J. Bot.*, 1982, **60**, 98–104.
63 A. S. Nezhad, M. Naghavi, M. Packirisamy, R. B. Bhat and A. Geitmann, *Proc. Natl. Acad. Sci. U. S. A.*, 2013, **110**, 8093–8098.
64 C. G. Agudelo, A. Sanati, M. Ghanbari, M. Packirisamy and A. Geitmann, *J. Micromech. Microeng.*, 2012, **22**, 115009.
65 C. G. Agudelo, A. S. Nezhad, A. S. Nezhad, M. Ghanbari, M. Naghavi, M. Packirisamy and A. Geitmann, *Plant J.*, 2013, **73**, 1057–1068.
66 A. Sanati Nezhad, M. Ghanbari, C. G. Agudelo, M. Naghavi, M. Packirisamy, R. B. Bhat and A. Geitmann, *Biomed. Microdevices*, 2014, **16**, 23–33.
67 *COMSOL Multiphysics® v. 6.4*, https://www.comsol.com, COMSOL AB, Stockholm, Sweden.
68 N. Yanagisawa, N. Sugimoto, H. Arata, T. Higashiyama and Y. Sato, *Sci. Rep.*, 2017, **7**, 1403.
69 A. K. Yetisen, L. Jiang, J. R. Cooper, J. Cooper, Y. Qin, R. Palanivelu and Y. Zohar, *J. Micromech. Microeng.*, 2011, **21**, 054018.
70 M. Horade, M. M. Kanaoka, M. Kuzuya, T. Higashiyama and N. Kaji, *RSC Adv.*, 2013, **3**, 22301–22307.
71 N. Yanagisawa and T. Higashiyama, *Biomicrofluidics*, 2018, **12**(2), 024113.
72 A. Nezhad, M. Packirisamy and A. Geitmann, *Plant J.*, 2014, **80**, 185–195.
73 N. Yanagisawa, E. Kozgunova and T. Higashiyama, *RSC Adv.*, 2021, **11**, 27011–27018.
74 C. Agudelo, M. Packirisamy and A. Geitmann, *Sci. Rep.*, 2016, **6**, 19812.
75 C. Hu, H. Vogler, M. Aellen, N. Shamsudhin, B. Jang, J. T. Burri, N. Läubli, U. Grossniklaus, S. Pané and B. J. Nelson, *Lab Chip*, 2017, **17**, 671–680.
76 K. S. Elvira, X. C. i Solvas, R. C. R. Wootton and A. J. deMello, *Nat. Chem.*, 2013, **5**, 905–915.
77 E. Moratto and G. Sena, *Bioelectricity*, 2023, **5**, 47–54.
78 A. S. Nezhad, M. Naghavi, M. Packirisamy, R. B. Bhat and A. Geitmann, *Lab Chip*, 2013, **13**, 2599–2608.
79 R. Benkert, G. Obermeyer and F.-W. Bentrup, *Protoplasma*, 1997, **198**, 1–8.
80 J. T. Burri, H. Vogler, N. F. Läubli, C. Hu, U. Grossniklaus and B. J. Nelson, *New Phytol.*, 2018, **220**, 187–195.
81 W. Kammerer and D. J. Cove, *Mol. Gen. Genet.*, 1996, **250**, 380–382.
82 M. J. Prigge and M. Bezanilla, *Development*, 2010, **137**, 3535–3543.
83 T. C. Merkel, V. I. Bondar, K. Nagai, B. D. Freeman and I. Pinnau, *J. Polym. Sci., Part B: Polym. Phys.*, 2000, **38**, 415–434.
84 C. S. Bascom, S.-Z. Wu, K. Nelson, J. Oakey and M. Bezanilla, *Plant Physiol.*, 2016, **172**, 28–37.
85 G. I. Jenkins and D. J. Cove, *Planta*, 1983, **157**, 39–45.
86 F. Furt, K. Lemoi, E. Tüzel and L. Vidali, *BMC Plant Biol.*, 2012, **12**, 70.
87 E. Kozgunova and G. Goshima, *Sci. Rep.*, 2019, **9**, 15182.
88 C. Grierson, E. Nielsen, T. Ketelaarc and J. Schiefelbein, *Arabidopsis Book*, 2014, vol. 12, DOI: 10.1199/tab.0172.
89 K. Yi, B. Menand, E. Bell and L. Dolan, *Nat. Genet.*, 2010, **42**, 264–267.
90 P. Denninger, A. Reichelt, V. A. F. Schmidt, D. G. Mehlhorn, L. Y. Asseck, C. E. Stanley, N. F. Keinath, J.-F. Evers, C. Grefen and G. Grossmann, *Curr. Biol.*, 2019, **29**, 1854–1865.e5.
91 S. Gilroy and D. L. Jones, *Trends Plant Sci.*, 2000, **5**, 56–60.
92 D. J. Gage, *Microbiol. Mol. Biol. Rev.*, 2004, **68**, 280–300.
93 A. H. N. Griffis, N. R. Groves, X. Zhou and I. Meier, *Front. Plant Sci.*, 2014, **5**, 129.
94 S. Zhang, J. Liu, X. Xue, K. Tan, C. Wang and H. Su, *Biochem. Biophys. Res. Commun.*, 2019, **519**, 783–789.
95 H. Wu, W. Liu, Q. Tu, N. Song, L. Li, J. Wang and J. Wang, *Microfluid. Nanofluid.*, 2011, **10**, 867–876.
96 T. Seidel, P. J. Artmann, I. Gkekas, F. Illies, A.-L. Baack and M. Viefhues, *Plants*, 2024, **13**, 295.
97 P. Durand-Smet, T. A. Spelman, E. M. Meyerowitz and H. Jönsson, *Proc. Natl. Acad. Sci. U. S. A.*, 2020, **117**, 17399–17408.
98 S. Xu, Z. Sun, L. Liu, H. Liu, Y. Yang, S. Zhang, Y. Li, N. Bao, Y. Zhang and L. Sun, *Processes*, 2022, **10**, 2507–2508.
99 J. Maisch, K. Kreppenhofer, S. Büchler, C. Merle, S. Sobich, B. Görling, B. Luy, R. Ahrens, A. E. Guber and P. Nick, *J. Plant Physiol.*, 2016, **200**, 28–34.
100 B. Zaban, W. Liu, X. Jiang and P. Nick, *Sci. Rep.*, 2014, **4**, 5852.
101 J. Park, D. Kurihara, T. Higashiyama and H. Arata, *Sens. Actuators, B*, 2014, **191**, 178–185.

102 K. Gooh, M. Ueda, K. Aruga, J. Park, H. Arata, T. Higashiyama and D. Kurihara, *Dev. Cell*, 2015, **34**, 242–251.
103 P. T. Kumar, F. Toffalini, D. Witters, S. Vermeir, F. Rolland, M. L. A. T. M. Hertog, B. M. Nicolaï, R. Puers, A. Geeraerd and J. Lammertyn, *Sens. Actuators, B*, 2014, **199**, 479–487.
104 Z. Yu, C. R. Boehm, J. M. Hibberd, C. Abell, J. Haseloff, S. J. Burgess and I. Reyna-Llorens, *PLoS One*, 2018, **13**, e0196810.
105 T. Galkovskyi, Y. Mileyko, A. Bucksch, B. Moore, O. Symonova, C. A. Price, C. N. Topp, A. S. Iyer-Pascuzzi, P. R. Zurek, S. Fang, J. Harer, P. N. Benfey and J. S. Weitz, *BMC Plant Biol.*, 2012, **12**, 116.
106 H. Jiang, X. Wang, T. M. Nolan, Y. Yin, M. R. Aluru and L. Dong, in *2017 IEEE 12th International Conference on Nano/Micro Engineered and Molecular Systems (NEMS)*, 2017, pp. 756–760.
107 X. Wang, H. Jiang, Y. Wang and L. Dong, in *2017 IEEE 12th International Conference on Nano/Micro Engineered and Molecular Systems (NEMS)*, 2017, pp. 398–401.
108 M. A. Buttkewitz, C. Heuer and J. Bahnemann, *Curr. Opin. Biotechnol.*, 2023, **83**, 102978.
109 H. Dai, B. Wu, B. Chen, B. Ma and C. Chu, *Environ. Sci. Technol.*, 2022, **56**, 9075–9082.
110 A. Rizza, B. Tang, C. E. Stanley, G. Grossmann, M. R. Owen, L. R. Band and A. M. Jones, *Proc. Natl. Acad. Sci. U. S. A.*, 2021, **118**, e1921960118.
111 V. Ghildiyal, C. M. Altaner, B. Heffernan and M. C. Jarvis, *Curr. For. Rep.*, 2025, **11**, 7.
112 D. Clarke, H. Whitney, G. Sutton and D. Robert, *Science*, 2013, **340**, 66–69.
113 M. Salvalaio, N. Oliver, D. Tiknaz, M. Schwarze, N. Kral, S.-J. Kim and G. Sena, *Plant Physiol.*, 2022, **188**, 1604–1616.
114 E. Moratto, Z. Tang, T. O. Bozkurt and G. Sena, *Sci. Rep.*, 2024, **14**, 19993.
115 Y.-S. Sun, *Sensors*, 2017, **17**, 2048.
116 C. E. Stanley, G. Grossmann, X. C. i Solvas and A. J. deMello, *Lab Chip*, 2016, **16**, 228–241.
117 P. M. Mafla-Endara, C. Arellano-Caicedo, K. Aleklett, M. Pucetaite, P. Ohlsson and E. C. Hammer, *Commun. Biol.*, 2021, **4**, 1–12.
118 B. Wang, H. Hou and Z. Zhu, *Geotech. Res.*, 2021, **8**, 130–138.
119 L. Paré, C. Banchini, C. Hamel, L. Bernier and F. Stefani, *Symbiosis*, 2022, **88**, 61–73.
120 D. Scheidweiler, A. D. Bordoloi, W. Jiao, V. Sentchilo, M. Bollani, A. Chhun, P. Engel and P. de Anna, *Nat. Commun.*, 2024, **15**, 191.
121 A. J. Clark, E. Masters-Clark, E. Moratto, P. Junier and C. E. Stanley, *Biomicrofluidics*, 2024, **18**, 054109.
122 D. Sarkar, Y. Sun, A. Tayagui, R. Adams, A. Garrill and V. Nock, in *2022 IEEE 35th International Conference on Micro Electro Mechanical Systems Conference (MEMS)*, 2022, pp. 884–887.
123 E. C. Hammer, C. Arellano-Caicedo, P. M. Mafla-Endara, E. T. Kiers, T. Shimizu, P. Ohlsson and K. Aleklett, *Fungal Ecol.*, 2024, **67**, 101302.
124 F. Richter, M. Calonne-Salmon, M. G. A. van der Heijden, S. Declerck and C. E. Stanley, *Lab Chip*, 2024, **24**, 1930–1946.
125 J. McGaley, B. Schneider and U. Paszkowski, *J. Microsc.*, 2025, **297**, 289–303.
126 J. Gao, J. Sasse, K. M. Lewald, K. Zhalnina, L. T. Cornmesser, T. A. Duncombe, Y. Yoshikuni, J. P. Vogel, M. K. Firestone and T. R. Northen, *J. Visualized Exp.*, 2018, e57170.
127 P. Suwanchaikasem, A. Idnurm, J. Selby-Pham, R. Walker and B. A. Boughton, *Plant Methods*, 2022, **18**, 46.
128 B. Gumuscu, *Lab Chip*, 2025, **25**, 3297–3313.
129 T. Finkbeiner, C. Manz, M. L. Raorane, C. Metzger, L. Schmidt-Speicher, N. Shen, R. Ahrens, J. Maisch, P. Nick and A. E. Guber, *Protoplasma*, 2022, **259**, 173–186.
130 C. A. Schneider, W. S. Rasband and K. W. Eliceiri, *Nat. Methods*, 2012, **9**, 671–675.
131 A. Kirillov, E. Mintun, N. Ravi, H. Mao, C. Rolland, L. Gustafson, T. Xiao, S. Whitehead, A. C. Berg, W.-Y. Lo, P. Dollár and R. Girshick, *arXiv*, 2023, preprint, arXiv:2304.02643, DOI: 10.48550/arXiv.2304.02643.
132 V. B. Koman, T. T. S. Lew, M. H. Wong, S.-Y. Kwak, J. P. Giraldo and M. S. Strano, *Lab Chip*, 2017, **17**, 4015–4024.
133 R. Soffe, M. Bernach, M. N. P. Remus-Emsermann and V. Nock, *Sci. Rep.*, 2019, **9**, 14420.
134 L. Jingmin, L. Chong, X. Zheng, Z. Kaiping, K. Xue and W. Liding, *PLoS One*, 2012, **7**, e50320.